This is a repository copy of *Co-seismic and rainfall-triggered landslide hazard susceptibility assessment for Uganda derived using fuzzy logic and geospatial modelling techniques*.

White Rose Research Online URL for this paper:
https://eprints.whiterose.ac.uk/215347/

Version: Published Version

Article:

ORIGINAL PAPER

Co-seismic and rainfall-triggered landslide hazard susceptibility assessment for Uganda derived using fuzzy logic and geospatial modelling techniques

Morris Oleng[1,2,3] **· Zuhal Ozdemir**[1] **· Kypros Pilakoutas**[1]

Abstract

Uganda has suffered from many damaging landslides like the 1966 Rwenzori, 1994 Kisomoro and 2010 Bududa events. Despite escalating landslide risks exacerbated by rapid deforestation, urbanization and population growth coupled with a substandard building stock, comprehensive national co-seismic and rainfall-induced landslide hazard and risk maps for Uganda do not exist. This study therefore aims to conduct landslide hazard assessment and zonation for Uganda using a geospatial-based fuzzy logic methodology. In this methodology, landslide frequency ratios obtained for the 1966 Toro and 1994 Kisomoro earthquakes are assigned to the stochastic event-based probabilistic seismic hazard map derived using *OpenQuake*-engine. The available co-seismic and rainfall-induced landslide inventory datasets are used to derive the distribution of landslide frequency ratios based on geology, topographic slope position index, slope aspect, slope angle, distance from streams, and proximity to major active faults. The spatial distribution of fuzzy membership functions obtained from frequency ratios are overlaid and aggregated to produce landslide susceptibility maps showing relative probabilities of landslide occurrences across Uganda. Results indicate that the highest overall landslide hazard susceptibility is expected in areas comprising highly weathered outcropping rocks of precambrian granites, dominantly metasedimentary, and granulites and gneisses geologies within 40 km from major active faults; where the bedrock peak ground acceleration ≥ 0.1 g, topographic position index ≥ 3.8, slope gradient $\geq 10°$, and the distance from streams ≤ 1.25 km. These findings can inform Uganda's directorate of disaster preparedness and management towards pioneering the development of co-seismic landslide risk mitigation measures for the country.

Keywords Uganda · Landslide inventory · Landslide conditioning factors · Fuzzy logic · GIS-based modelling · Stochastic event-based modelling · Landslide zonation and susceptibility mapping

Extended author information available on the last page of the article

🍃 Springer

1 Introduction

Over the past few decades, Uganda has experienced an increasing frequency of landslide events due to the escalating rates of deforestation, urbanisation and population growth. Landslides in Uganda, which have mostly occurred in the mountainous areas (Nakileza and Nedala 2020), have resulted in numerous deaths, injuries and damage to the ecosystem, services and infrastructure (Masaba et al. 2017). Uganda's National Planning Authority reported in its development plan that landslide occurrences between 1933 and 2012 were responsible for approximately 14% of the country's socio-natural disaster related deaths (Akera 2012), with over 4% of the population grossly affected due to past landslides (Doocy et al. 2013; Kato and Mutonyi 2011; Vlaeminck et al. 2016). Nationally, over 250 people are annually exposed to landslide risk, with a long term mean annual fatality estimate of 20 persons; and according to Uganda's recent disaster risk profile, the expected average annual damage to the building stock falls in excess of US$ 850,000, in addition to over US$ 200,000 estimated as the combined average cost of damage to education centres and healthcare facilities each year (WorldBank 2019).

Various previous studies indicate that landslides across Uganda are largely induced by rainfall and earthquakes (Knapen et al. 2006; Nefeslioglu et al. 2011). In general, rainfall-triggered landslides have been observed around Mount Elgon in Eastern Uganda. In March 2010, a rainfall-induced landslide occurred in Bududa district in eastern Uganda and killed at least 388 people, with more than 8500 lives affected (Broeckx et al. 2019; Mugagga et al. 2012; Wanasolo 2012). Moreover, earthquake-induced secondary effects such as landslides can considerably aggravate the overall damages, injuries and loss of lives (Chousianitis et al. 2016). Within Uganda's territory, regions surrounding the Rwenzori Mountains in western Uganda are exposed to earthquake-triggered landslides due to their tectonic environment, seismicity, topography, geomorphology and geology (Jacobs et al. 2016). For example, the 1966 Toro and 1994 Kisomoro earthquakes with surface wave magnitude (M_s) of 6.6 and 6.2, respectively, triggered numerous co-seismic landslides in Bundibugyo, Kasese, Kabarole and Bunyangabu districts of western Uganda (Sykes 1967; UNESCO 1966; USGS 2010). Except for Kampala capital city and its immediate environs, these regions comprise some of the most populated areas of Uganda.

Landslide hazard and risk analyses typically encompass the utilization of suitable methods to assess complex geo-physical processes. Several methods proposed in literature have been used to assess landslide susceptibility, inventory mapping, hazard prediction and evaluation of the associated landslide risks (Aleotti and Chowdhury 1999). To begin with, different approaches have been categorised on the basis of assessment area units. Although the assessment area units may be automatically derived from overlays of each landslide parameter map (Ives and Bovis 1978), regular grids of identical size and shape (Anbalagan and Singh 1996; Carrara 1983) and/or individual hillslopes and other morphological units (Carrara et al. 1992; Kienholz 1978) can alternatively be adopted. In contrast, landslide assessment procedures can be categorised into relative hazard, statistical or deterministic absolute hazard, empirical hazard, and monitored landslide hazard (Hartlen and Viberg 1988).

On a broader perspective, landslide hazard assessment can be categorised to consist of qualitative and quantitative approaches. Previous studies (e.g., Bughi et al. 1996; Carrara and Merenda 1976; Fenti et al. 1979; Gupta and Anbalagan 1997; Hearn 1995; Ives and Messerli 1981; Rupke et al. 1988; Soeters and Van Westen 1996) utilized qualitative techniques to assess landslides. Conversely, quantitative landslide assessment techniques

essentially involve the interpretation of empirical data to evaluate both triggering (causative) and conditioning (preparatory) factors associated with landslides. Whereas the temporal distribution of slope movement is governed by the triggering factors (e.g., rainfall, earthquakes, volcanic eruptions, human activity, and rapid snowmelt), landslide conditioning parameters such as geology, topography, hydrology, environmental and meteorological aspects are linked with the spatial distribution of landslide occurrences (Hervás and Bobrowsky 2009). To conduct a quantitative landslide susceptibility assessment, statistical, geotechnical and/or neural network analyses can be employed.

In statistical analysis, weighted values are attributed to several landslide conditioning factors and the spatial distribution of landslides compared with each factor considered in the analysis, either in a bivariate or multivariate manner (Aleotti and Chowdhury 1999; Baeza and Corominas 1996; Clerici and Dall'Olio 1995; Leroi 1996; Wieczorek et al. 1996). Regarding geotechnical approaches, either a deterministic framework which involves quantifying the soil properties and calculating the factor of safety (Aleotti and Chowdhury 1999; Chowdhury and Bertoldi 1977) or probabilistic methods that further account for the magnitude-time variability of undrained shear strength, angle of internal friction and cohesion (Chowdhury 1984; Nguyen and Chowdhury 1984) can be applied. On the other hand, neural networks (black box model) suggested by Lees (1996) can be used for landslide hazard assessment. The application and further descriptions of quantitative methods for landslide hazard assessment can be found in literature (e.g., Aleotti et al. 1998; Bortolami et al. 1994; Carrara 1983; Choubey et al. 1992; Kingsbury et al. 1992; Meherota et al. 1994).

The upsurge in human and economic losses due to previous landslides across Uganda has prompted several studies over recent decades. Knapen et al. (2006) used statistical methods to investigate rainfall-induced landslides in the densely populated Manjiya County located at the foot slopes of Mount Elgon. The results indicated dominant landslides on steep concave slopes of northeast orientation. Besides, landslides along such slopes were exacerbated by human interferences like deforestation, unsuitable agricultural practices and foundation excavations along unstable hillslopes (Kitutu et al. 2009, 2011). In another study characterizing the physical properties and occurrence of major rainfall-triggered landslides on the slopes of Mount Elgon, Mugagga et al. (2012) indicated that the soils are inherently prone to landslides, even without human intervention. Likewise, Bamutaze (2019) analysed 286 georeferenced rainfall-induced landslides from which the catchment area around Mount Elgon was delineated, and morphometric and terrain attributes extracted from a 33-m digital elevation model (DEM). Results showed the highest landslide frequency along middle segments at predominantly 1500–1900 m above sea level (m.a.s.l) and 10–30° gradients.

In their study of the upper Manafwa catchment located in eastern Uganda, Nakileza and Nedala (2020) used landslide inventory data, field surveys and a 30-m DEM to characterise and statistically determine frequency ratios for the most dominant topographic factors responsible for landslides in the area. The spatial distribution of landslides revealed that mid to upper slope positions (altitude ranging 1500–1800 m.a.s.l) of moderately steep gradients between 15 and 20° were most susceptible to landslides. Moreover, it was noted that human encroachment onto critical slopes often triggered shallow and deep landslides (Broeckx et al. 2019). In another study, Jacobs et al. (2017) assessed the characteristics and spatial distribution of both rainfall- and earthquake-triggered landslides covering a catchment area of 114 km^2 around the Rwenzori Mountains. The results showed the highest concentration of both rainfall-induced and co-seismic landslides on slope gradients of 10–15° and 25–30° along the lowlands (< 1500 m.a.s.l)

and highlands (1500–5109 m.a.s.l) respectively. Nseka et al. (2019) relied on field surveys and a 10-m DEM to statistically evaluate the topographic parameters inducing landslides in the Kigezi region of south-western Uganda. The results revealed dominant occurrences in zones where slope gradients range between 25 and 35°.

Despite the vast spatial distribution of landslides across Uganda, many previous studies, except the attempt by Musinguzi and Asiimwe (2014), have only focused on landslide occurrences in the most critically struck regions of the country. Moreover, these previous studies have largely focused on Uganda's susceptibility to rainfall-triggered slope failures, without accounting for earthquake-induced landslides which struck the country's mountainous regions. Yet, the categorisation and discrimination of regions threatened by earthquake-induced landslides (e.g., using the GIS-based spatial multicriteria approach) is paramount towards building community resilience (Karpouza et al. 2021). This study, therefore, aims to conduct a holistic landslide susceptibility assessment and a comprehensive relative hazard zonation for Uganda. Using the *OpenQuake*-engine (Pagani et al. 2014), a fault-oriented spatially smoothed seismicity technique (Pagani et al. 2023; Weatherill 2014) is employed to model earthquake characteristics. A subsequent assessment of rainfall and earthquake-triggered landslides across Uganda is then performed using a fuzzy logic approach that is implemented in *ArcGIS* (Raines et al. 2010) environment. Predominant landslide conditioning factors (e.g., topography, lithology and hydrology) are analysed in conjunction with rainfall and earthquake triggering factors to produce a comprehensive relative landslide hazard susceptibility map for Uganda.

2 Fuzzy logic method for landslide hazard assessment

Fuzzy logic approach, initially introduced by Zadeh (1965), can be used to assess the likelihood of landslides in an area by assuming that the factors responsible for inducing past landslides can reliably be used as indicators for triggering future events occurring within the same region (Anbalagan et al. 2015; Lee and Talib 2005; Tangestani 2004). As opposed to alternative methods of landslide susceptibility assessment, the GIS-based fuzzy logic approach is employed for regions with scarce landslide inventory. For instance Gorsevski et al. (2003), Kanungo et al. (2009), Kayastha (2012), Tangestani (2004) and Kritikos et al. (2015) employed the fuzzy logic approach to predict the distribution of landslides across various global catchments. This procedure involves determining landslide frequency ratios, deriving semi-data driven fuzzy memberships and fuzzy maps for the different conditioning factors, and implementing the fuzzy overlay tools to produce landslide susceptibility maps. The schematic diagram illustrating the sequential workflow of fuzzy logic approach implemented in *ArcGIS* (Raines et al. 2010) environment is presented in Fig. 1.

Herein, a statistical bivariate method (Aleotti and Chowdhury 1999; Leroi 1996) is used to calculate the spatial relationship between the location of landslides and landslide conditioning (geology, topographic slope position index, slope aspect, slope angle, distance from streams and proximity to active faults) as well as triggering factors (earthquakes). The frequency ratio (FR_i) is defined as the ratio of the frequency of landslides within a specific conditioning and/or triggering factor class i to the relative frequency of all observed landslide pixels across the study area (Lee and Pradhan 2007; Lee and Sambath 2006; Yilmaz 2009). This is expressed as:
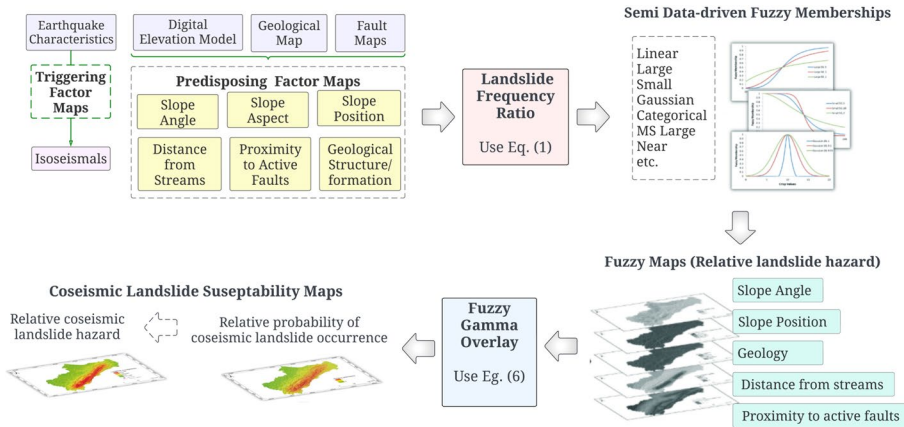
Fig. 1 Schematic illustration of the GIS-based fuzzy logic method employed to produce co-seismic landslide susceptibility maps for Uganda

$$FR_i = \frac{N_{(P)i}/N(P)}{N(LP)/N_T} \tag{1}$$

where $N_{(P)i}$ is the number of observed landslide pixels (unit area) in a landslide factor category i, $N_{(P)}$ is the total number of pixels in the selected factor category i, $N_{(LP)}$ is the total number of observed landslide pixels in the region of interest, and N_T is the total number of pixels in the entire study area. The approach defined in Eq. 1 is adopted because the landslide scars obtained are captured as raster images which support pixel counts in *ArcGIS* (Raines et al. 2010).

Following the determination of landslide frequency ratios for each landslide parameter, the fuzzy membership functions (e.g., *Linear, Large, Small, Gaussian, Categorical, MS Large,* and *Near*) available in the fuzzy membership tool embedded in *ArcGIS* (Raines et al. 2010) are implemented to produce fuzzy maps; prior to the application of fuzzy overlay operators used to generate membership functions and landslide conditioning parameter maps for the various landslide conditioning factors (Bonham-Carter 1994; Wang et al. 2009). Landslide conditioning parameter maps are then aggregated and their spatial distribution overlaid to produce the final fuzzy sets describing the relative co-seismic landslide hazard susceptibility for the region in question (Dubois and Prade 1985; Kayastha 2012; Zimmermann 2012). The fuzzy algebraic *OR*, fuzzy algebraic *AND*, fuzzy *PRODUCT*, fuzzy *SUM*, and fuzzy *GAMMA* are defined as follows:

$$\text{Fuzzy } OR \ \mu(x) = \max(\mu_i) \tag{2}$$

$$\text{Fuzzy } AND \ \mu(x) = \min(\mu_i) \tag{3}$$

$$\text{Fuzzy } SUM \ \mu(x) = 1 - \prod_{i=1}^{n}(1 - \mu_i) \tag{4}$$

$$\text{Fuzzy } PRODUCT \ \mu(x) = \prod_{i=1}^{n} \mu_i \tag{5}$$

$$\text{Fuzzy } GAMMA \ \mu(x) = \left[1 - \prod_{i=1}^{n} (1 - \mu_i) \right]^{\gamma} \times \left[\prod_{i=1}^{n} \mu_i \right]^{1-\gamma} \tag{6}$$

where $\mu(x)$ is the combined membership function, μ_i is the fuzzy membership function for the *ith* fuzzy overlay map, and the parameter γ is chosen in the range of 0 and 1. The γ-value establishes the effect of large μ_i values (fuzzy membership functions favouring the occurrence of landslides) compared to small μ_i values (fuzzy membership functions discouraging landslide occurrence). Therefore, at known landslide locations like in Bududa and Manafwa districts located around Mount Elgon in eastern Uganda, it is expected that the optimal value of γ will predict high hazard levels (Kritikos et al. 2015).

3 Case study area: Uganda

Uganda is a Sub-Saharan African country which lies along the equator between latitude: 1º S and 4º N, and longitude: 30º E and 35º E, as shown in Fig. 2a. The country has a total area of 241,550 km², of which 41,027 km² (approximately 17%) is open inland water. Majority of the country's territory receives mean annual rainfall between 1000 and 1500 mm. An average annual population growth rate of 3.19% has been recorded over the past few years and as at June 2022, Uganda's population stood at over 44.2 million (UBoS 2022). The landlocked East African country sits at an estimated average altitude of 900 m.a.s.l and comprises a diverse geography of lakes, mountains and volcanos. The first elevation data
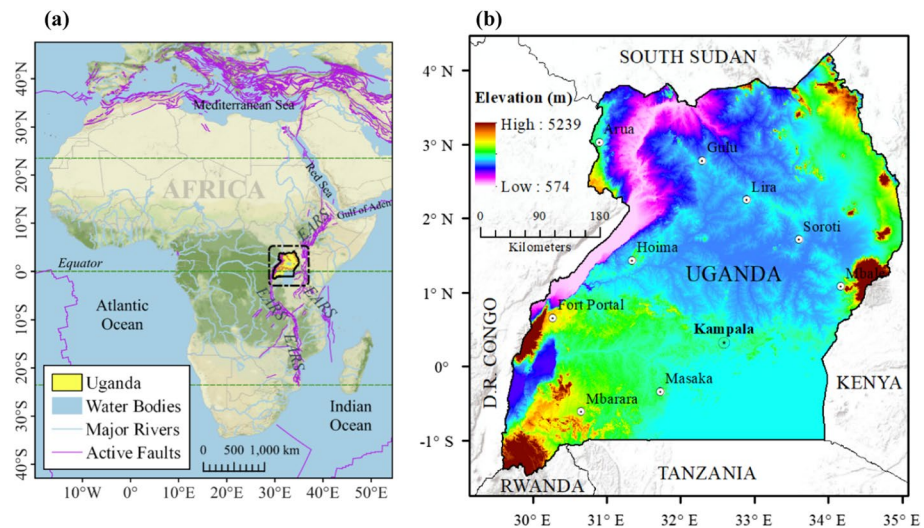

Fig. 2 **a** Uganda's geographical location between the two arms of the East African Rift System, superimposed on the African continent; and **b** Map of the study area showing regional cities and the 30-m Shuttle Radar Topography Mission digital elevation model

compiled between 1962 and 1970 is obtained locally from National Forest Authority and merged with the 30-m Shuttle Radar Topography Mission (RCMRD 2022; USGS 2022a) as depicted in Fig. 2b. The major areas that are largely prone to rainfall-induced and co-seismic landslides include:

1. The Rwenzori Mountains, situated along the equator crossing the western arm of the East African Rift System (EARS) shown in Fig. 3, are amongst the country's most remarkable highlands. Mount Rwenzori is a peninsular raising to a maximum of 5109 m.a.s.l and it comprises an active seismo-tectonic setting (Koehn et al. 2010), gneisses geology (Bauer et al. 2012), ecology (Eggermont et al. 2009), glaciers (Taylor et al. 2009) and long-term soil erosion processes (Roller et al. 2012). Because of its geomorphology, regions around the Rwenzori Mountains have over the past experienced landslides of varying degrees. For instance, the densely populated districts of Kasese and Bundibugyo registered many human and economic losses due to previous landslides. However, limited scientific information is published regarding co-seismic landslides; except the studies conducted by Mavonga (2007), Eggermont et al. (2009) and Jacobs et al. (2017).
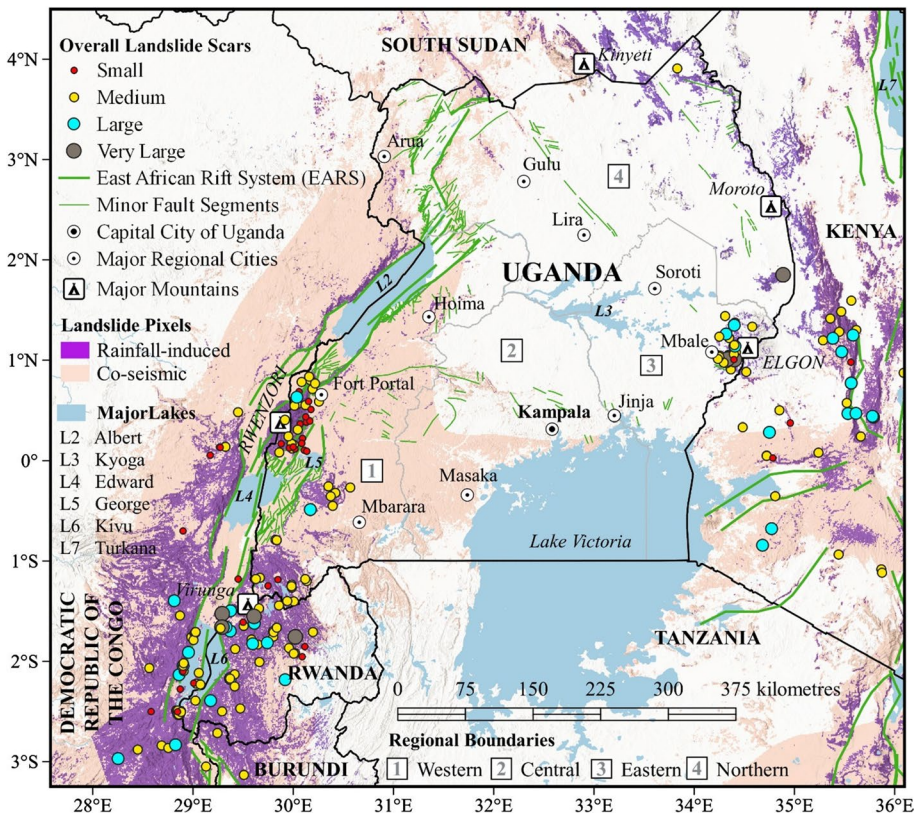

Fig. 3 Co-seismic and rainfall-induced landslide pixels (areas); relative to the major regional cities, active and minor fault systems, mountains and locations of known landslide scars which occurred in Uganda and around its neighbouring countries between 1933 and 2018

2. Mount Elgon, located in Eastern Uganda (see Fig. 3), is Uganda's most landslide-prone area. It is an extinct volcanic shield with a maximum elevation of 4321 m.a.s.l and predominantly characterized by weathering and intense precipitation along its steep cliffs (Knapen et al. 2006; Scott 1998). Partly due to its fertile soils, the human population of the area is quite high; with settlements spread on crests, hillslopes and valleys. This has led to increased losses during previous rainfall-induced landslides and rockfalls along the lower flanks of the volcano, especially in Bududa district (Broeckx et al. 2019; Knapen et al. 2006). More comprehensive descriptions of the geology, soils, land use and biodiversity of Mount Elgon can be found in literature (e.g., Simonetti and Bell 1995; Sassen et al. 2013; Van Eynde et al. 2017; Kitutu et al. 2009; Mugagga et al. 2012).

4 Landslide and earthquake datasets for Uganda

4.1 Landslide locations and pixel distribution

The landslide locations showing rainfall-induced and co-seismic landslide scars are acquired from National Aeronautics and Space Administration satellite repository (NASA 2022). Additional information on earthquake-triggered landslides is obtained from the US Geological Survey database (USGS 2022b). On the other hand, landslide pixel data is obtained from the World Bank and the Global Facility for Disaster Reduction and Recovery databases (WorldBank and GFDRR 2022). Subsequently, overall landslide scars are mapped on co-seismic and rainfall-induced landslide pixels as portrayed in Fig. 3, and the major active fault system indicated is taken from the Global Earthquake Model foundation database (Styron and Pagani 2020). It is observed that the mountainous parts of the country, especially Elgon and Rwenzori mountains, have experienced greater concentrations of landslide clusters compared to the other parts of the region. The concentration of landslides in these regions is partly due to unstable landscapes, in particular slope positions (Regmi et al. 2014).

4.2 Earthquake characteristics

Landslide frequency ratios and fuzzy membership functions are derived for two major events: 5th February 1994 Kisomoro (6.2 M_s) and 20th March 1966 Toro (6.6 M_s) earthquakes which struck the Rwenzori region in western Uganda (see Fig. 4a-b) at hypocentral depths of 14.2 and 29.3 km, respectively (Jacobs et al. 2017; Marano et al. 2010; Tanyaş et al. 2017). These events triggered extensive landslides around their epicentres. For instance, 0.1–1.0 km^2 of the relatively low-populated remote countryside was exposed to landslides in the aftermath of the 1966 Toro earthquake (USGS 2022b). In this work, landslide hazard analysis is incorporated into an existing seismic hazard model for Uganda. The 30-m average shear wave velocity and site-specific hazard maps for a 475-year return period are shown in Fig. 5a-b, in addition to seismic hazard maps on reference rock site conditions for 475-year and 2475-year return periods shown in Fig. 6a-b, respectively. Information on the existing stochastic event-based probabilistic seismic hazard analysis for Uganda can be found in the literature by Oleng et al. (2024).
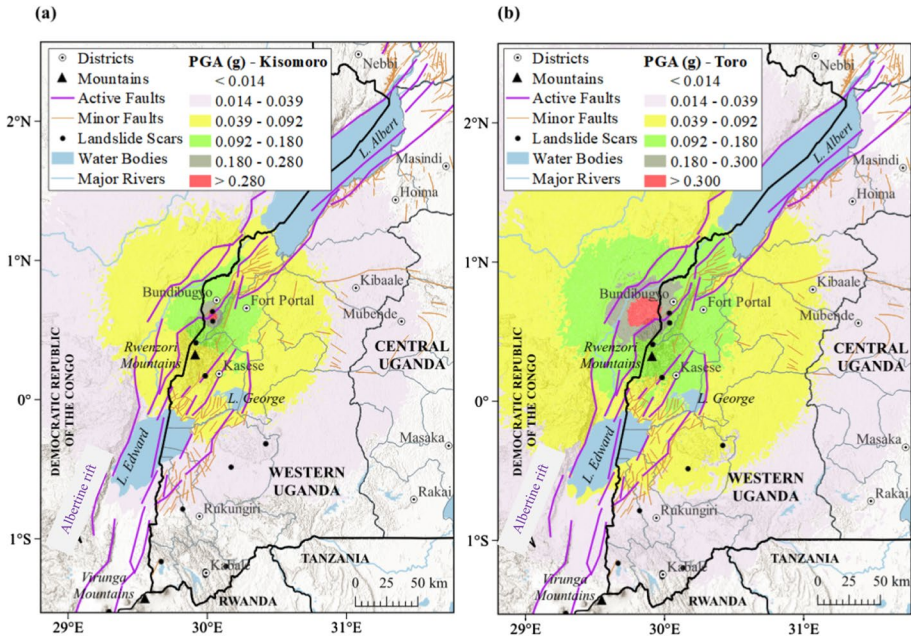
Fig. 4 Seismic hazard maps in terms of peak ground acceleration (PGA [g]) for scenario earthquakes: **a** the 5th February 1994 Kisomoro (6.2 M$_s$), and **b** the 20th March 1966 Toro (6.6 M$_s$)
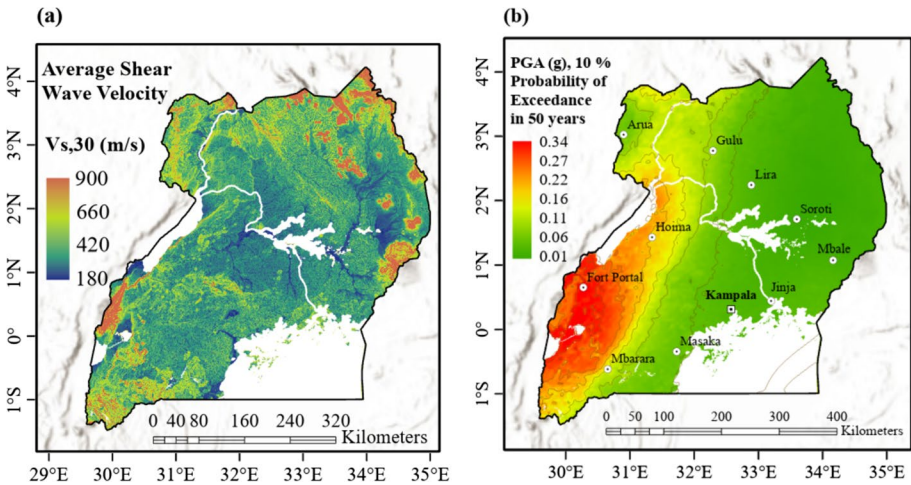

Fig. 5 **a** 30-m average shear-wave velocity reference map of Uganda, and **b** site-specific seismic hazard map in terms of PGA (g), with contour lines imposed at a 0.05 g interval and presented for a 475-year return period (Oleng et al. 2024)
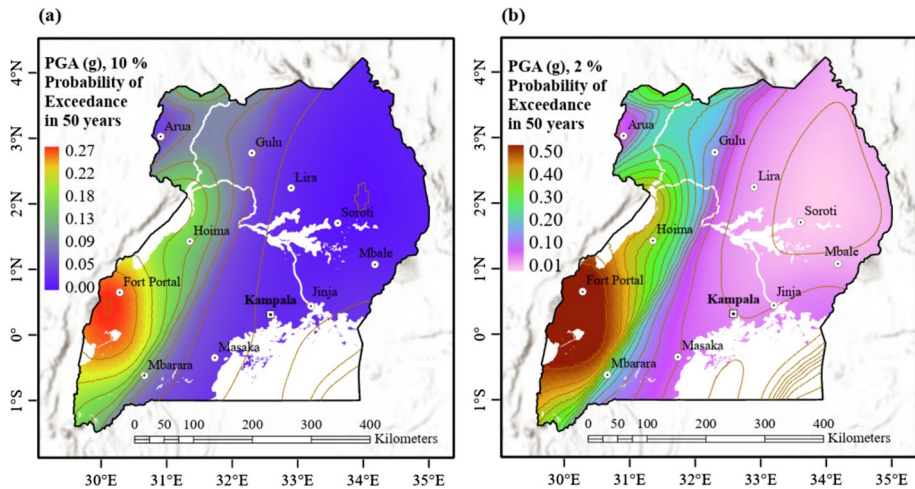
Fig. 6 Seismic hazard maps on reference rock site conditions in terms of PGA (g), with contours imposed at a 0.03 g interval, for: **a** 475-year return period, and **b** 2475-year return period (Oleng et al. 2024)

5 Landslide inventory analysis and model design

Historical landslide inventories can be used to represent future landslide susceptibility for a given region. However, many countries in the global south lack accurate and complete data relating to landslide susceptibility and inventories (Xu 2015). That notwithstanding, meaningful quantitative landslide hazard analyses are often performed based on triggering and conditioning parameters. The major landslide triggering parameters considered in this work include rainfall and earthquakes; which are modelled together lithology (geology, tectonics and topography) and hydrologic conditioning factors. The following sub-sections explain how the selected triggering and conditioning factors are designed and incorporated herein.

5.1 Triggering factors

Co-seismic landslides are often initiated when a rock/soil mass is subjected to strong ground motion, commonly quantified directly in terms of peak ground acceleration (PGA) or expressed indirectly in terms of the Modified Mercalli Intensity (MMI) scale (Baker et al. 2021; Kramer 1996; Kritikos et al. 2015). In this study, two earthquakes (the 1966 Toro and 1994 Kisomoro events) whose ground motion responses are shown in Fig. 4a-b are considered. In addition to the standard groupings of the MMI scale, frequency ratios are evaluated in terms of the following PGA (g) ranges: <0.014, 0.014–0.039, 0.039–0.092, 0.092–0.18, 0.18–0.28, and 0.28–0.36.

5.2 Conditioning parameters

5.2.1 Geology

Extensive variations on the geological timescale of Uganda have been recorded for over three billion years (Maasha 1975; Westerhof et al. 2014). The simplified geological map of
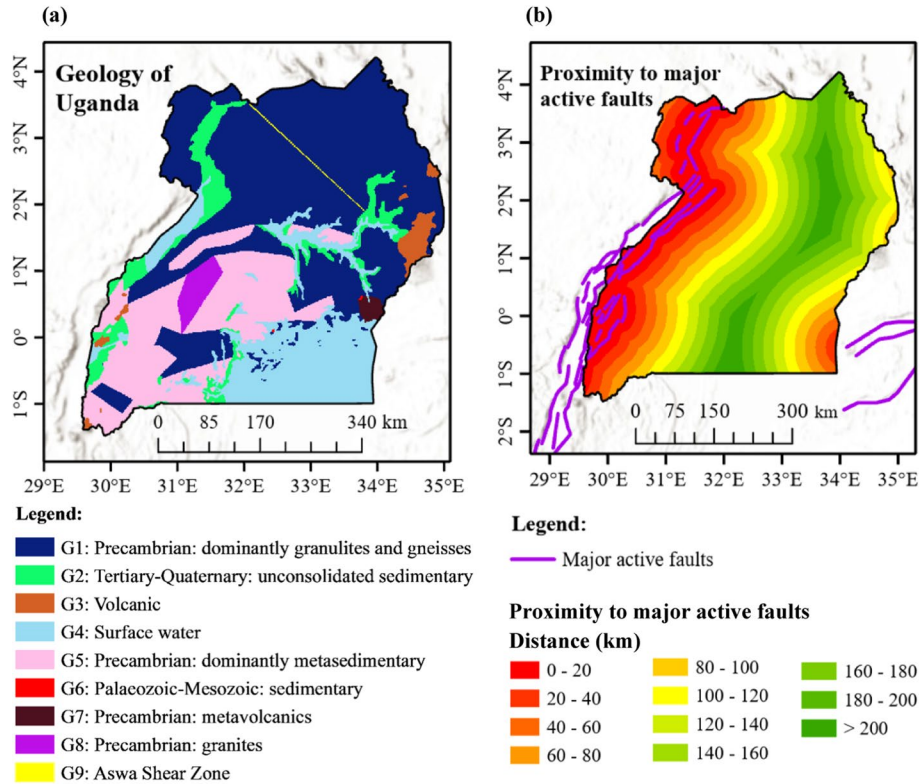
Fig. 7 Landslide conditioning factor maps of Uganda showing the inventory model characterisation for: **a** generalised geological formations, and **b** proximity to active faults

Uganda presented in Fig. 7a shows that the country largely comprises of Precambrian basement that is dominantly granulites and gneisses, metasedimentary, metavolcanics and granites. The other parts comprise Tertiary-Quaternary unconsolidated sedimentary geology. Along with Palaeozoic-Mesozoic sediments, across the country lies the volcanic region around the western and eastern boarders. Another geo-tectonic structure is the *Aswar* shear zone which is broadly stable and seismically inactive; except at its northern end where it intercepts the East African Rift System (Fairhead and Stuart 1982; Furman et al. 2006; Karp et al. 2012; McDougall and Brown 2009; Muwanga et al. 2001; Schlüter 2008; Sykes and Landisman 1964; Westerhof et al. 2014).

5.2.2 Proximity to the major active faults

Owing to various soil/rock weakening mechanisms like fault slip, geochemical alterations, and groundwater infiltration (Korup 2004; Warr and Cox 2001), the release of seismic energy along active faults may substantially reduce material strengths within a few kilometres of the lithosphere (Brune 2001; Dramis and Sorriso-Valvo 1994; Kellogg 2001; Kramer 1996). Due to considerable loss of material strength, the regions closer to active faults are more vulnerable to earthquake-triggered landslides (Petley 2012). While taking into account the minimum distance between faults and the maximum distance at which

landslide scars are mapped, a class size of 20 km is used to group distances from active faults in Uganda as shown in Fig. 7b. It is obvious that areas near the western boarder are much closer to the East African Rift System compared with the rest of the country, except for the eastern boundary which lies within a few kilometres from the eastern or Gregory arm of the East African Rift System.

5.2.3 Topographic slope position

Various hillslope types (e.g., valleys, mid-slopes and ridges) respond differently to earthquake-induced ground shaking (Athanasopoulos et al. 1999; Davis and West 1973; Havenith et al. 2003; Spudich et al. 1996). This is because of the localised increase in the amplitude of ground motion due to seismic wave propagation through the Earth's crust (Lee et al. 2009; Meunier et al. 2008; Wald and Allen 2007). This work utilises the Topographic Position Index (TPI), defined by Weiss (2001), to classify the land formation (morphology) across Uganda into discrete categories based on their relative slope positions. Within a predetermined neighbourhood, for instance a 10–15 cell size (300–500 m for small-scale TPI) and a 62–67 cell size (1.86–2.1 km for large-scale TPI), the TPI essentially measures the difference between the elevation of a given central point and the mean altitude of the surrounding grid cells. This is expressed as follows:

$$TPI = Z_o - \frac{\sum_{n-1} Z_n}{N} \tag{7}$$

where Z_o and Z_n respectively denote elevation at the central point and altitude of surrounding cells within a local window, and N is the total number of surrounding points employed in the evaluation. Positive TPI values indicate that the point under consideration is located at a higher altitude than its average surroundings, and vice versa. It is worth noting that whilst large-scale TPI values largely reveal major landscape units, smaller morphological features such as minor ridges and valleys are highlighted for small-scale TPI values (Drăguţ and Blaschke 2006; Jenness 2006; Weiss 2001). In this regard, small-scale predetermined neighbourhood of a 300-m grid/cell radius is considered herein and Uganda's landscape is subsequently categorised into 6 classes: valley, lower slope, flat slope, middle slope, upper slope and ridge (Jenness et al. 2013). According to Bufalini et al. (2021), the morphological categories shown in Fig. 8 are defined based on the range of TPI values presented in Table 1.

From the slope position map shown in Fig. 9a, majority of Uganda's territory consist of lower slopes, with the western and eastern boundaries predominantly comprising flat and

Fig. 8 Slope position classification obtained from topographic position index (Weiss 2001) used to generate the 6 topographic slope position classes used in this study
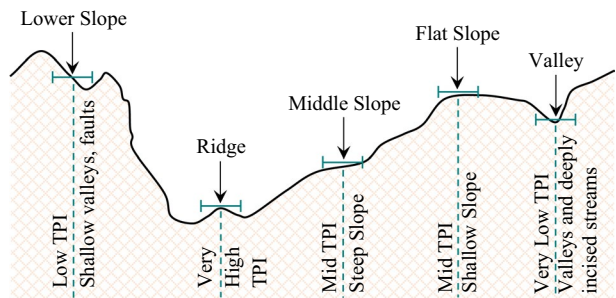
Table 1 Topographic position index (TPI) values corresponding to the various morphological features describing land form classes adopted for characterising slope positions across Uganda

Morphological classes	Range of TPI values	
	Lower limit	Upper limit
Valley (U-shaped valley/Spread water), deeply incised streams	− 63.5	− 13.3
Lower slope, shallow valleys, faults	− 13.3	− 4.3
Flat slope	− 4.3	3.8
Middle slope	3.8	13.8
Upper slope, small hills	13.8	28.8
Mountain tops, high ridges	28.8	64.5

middle slopes. Whereas the Albertine rift and West Nile block are mainly composed of valleys, upper slopes and ridges are largely observed around Uganda's mountainous regions.

5.2.4 Slope aspect

In landslide hazard zonation, slope orientation with respect to the North may be considered as a vital parameter (Kanungo et al. 2009; Nagarajan et al. 1998; Saha et al. 2002). This is because the effect of soil moisture content, air dryness and solar heating are determined by the slope aspect influence (Capitani et al. 2013; Cellek 2021; Yalcin 2008). It is worth noting that due to its triggering effect on precipitation, slope aspect is often evaluated in combination with other factors considered in this study (Ahmed 2015; Ayalew and Yamagishi 2005; Pachauri and Pant 1992). Moreover, the influence of slope aspect on vegetation cover and moisture retention can affect material shear strengths, and possibly initiate slope failure (Silalahi et al. 2019). Slope aspect can be classified in several ways depending on the purpose at hand (Bourenane et al. 2015; Caniani et al. 2008; Tangestani 2004). In this study, the slope aspect map shown in Fig. 9b is generated for 8 classes: north (0–22.5°, 337.5–360°), northeast (22.5–67.5°), east (67.5–112.5°), southeast (112.5–157.5°), south (157.5–202.5°), southwest (202.5–247.5°), west (247.5–292.5°) and northwest (292.5–337.5°).

5.2.5 Slope angle

Landslide incidences are substantially affected by slope angle, which is considered as a critical topographic parameter in the initiation of slope failures (Dahal et al. 2009; Gupta et al. 2008; Jibson et al. 2000; Kanungo et al. 2006). Steeper slopes are more susceptible to failure due to their greater vertical components of gravity which result in increased shear stresses within the soil (Kritikos et al. 2015). Hence, it is anticipated that steeper slopes subjected to significant ground motion will experience more landslides compared to gentle slopes. Accordingly, slope angles for the study region are categorized into 10 slope classes of 5° increments up to 50°, and a further class > 50° as shown in Fig. 9c. It is seen that most parts of the country generally lie within slope angles < 15°, except for the highland regions around Mount Elgon and Rwenzori ranges (see Fig. 3) where greater slopes angles are observed.
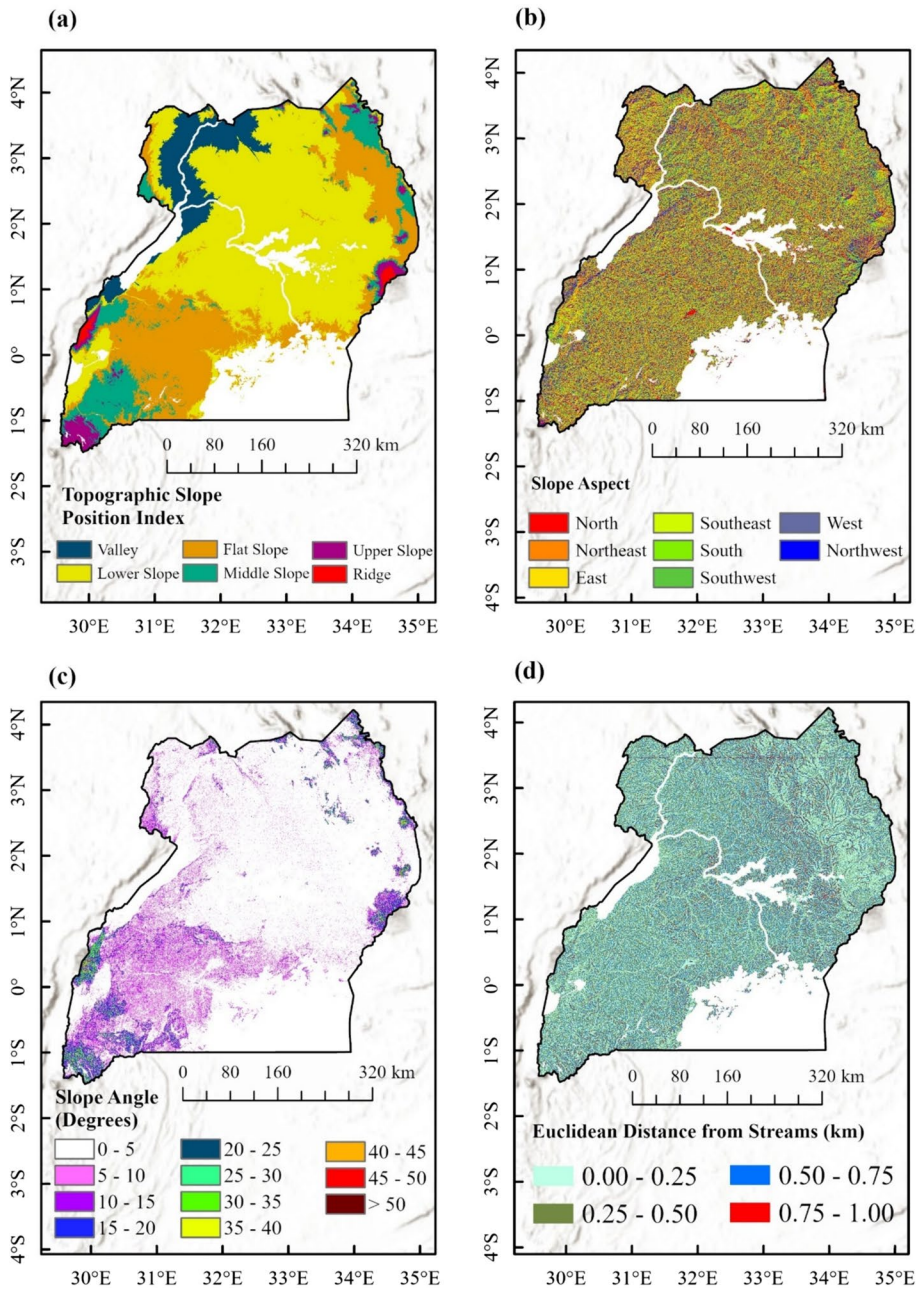
Fig. 9 Landslide conditioning parameter maps of Uganda, represented in terms of: **a** topographic slope position index, **b** slope aspect, **c**, slope angle, and **d** distance from streams

5.2.6 Distance from streams

Hydrological processes are significant in landscape evolution and as such various land-slide hazard studies have incorporated distance from drainage networks amongst the critical conditioning factors (Bathrellos et al. 2021; Larsen and Montgomery 2012; Snyder et al. 2000; Whipple 2004). The inclusion of hydrology not only takes into account the undercutting stream flow and terrain modification, but also stream channel and gulley erosion. These localised processes can progressively lead to the removal of horizontal restraints, thereby increasing shear stresses in the soil; a phenomenon which may eventually lead to induction of slope instability in the event of an earthquake (Dai et al. 2011; Donati and Turrini 2002; He and Beighley 2008; Korup 2004; Van Westen et al. 2003b). Based on the density of Uganda's drainage network, distances from streams are grouped into the following 8 classes: 0–0.25, 0.25–0.50, 0.50–0.75, 0.75–1.00, 1.00–1.25, and > 1.25 km. The map shown in Fig. 9d indicates the distribution of land-slide pixels with regard to their proximity to natural stream networks.

6 Results

6.1 Landslide frequency ratio

6.1.1 The 1966 Toro and 1994 Kisomoro earthquakes

Landslide frequency ratios for the 1966 Toro and 1994 Kisomoro events, whose characteristics are described in Sect. 4.2, are computed and plotted against landslide conditioning parameter classes in terms of MMI scale and PGA as shown in Fig. 10a-b. At a minimum, earthquakes of intensity exceeding MMI (II-III) and/or PGA > 0.05 g are capable of inducing landslides.
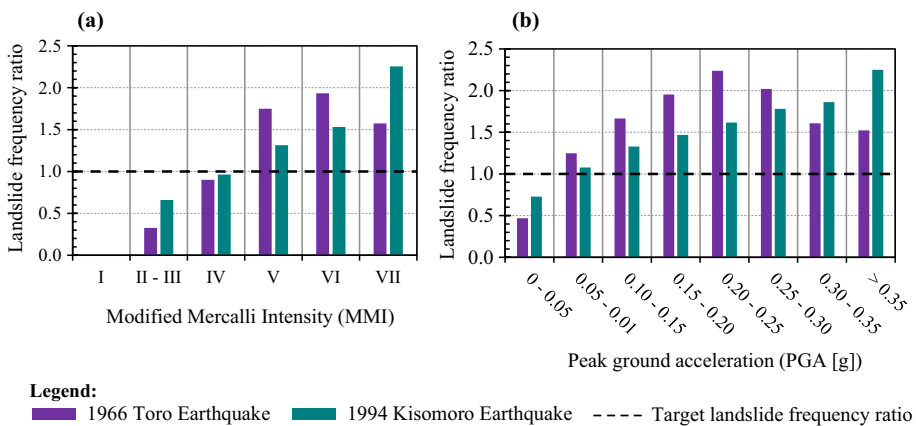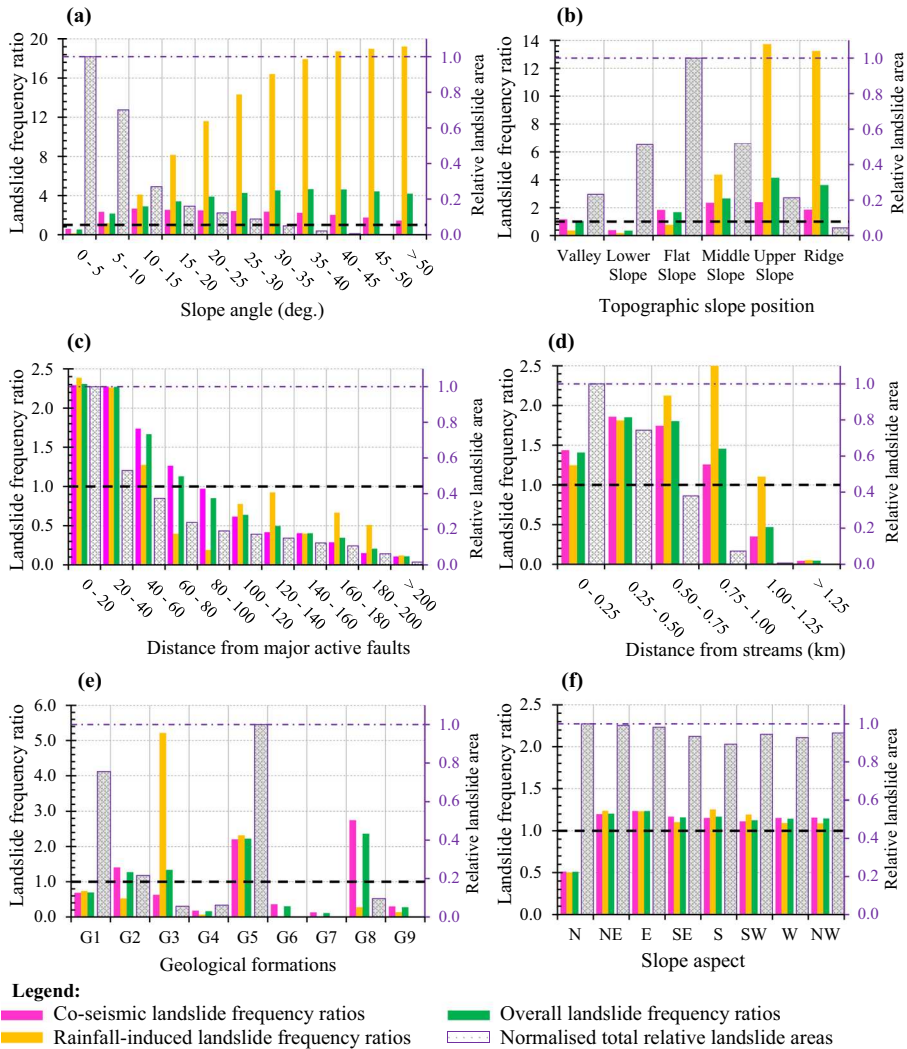

Fig. 10 Landslide frequency ratio for the 1966 Toro and 1994 Kisomoro earthquakes assessed in terms of: **a** Modified Mercalli Intensity (MMI) scale, and **b** Peak ground acceleration (PGA [g])

Fig. 11 Landslide frequency ratios obtained from co-seismic, rainfall-induced, and both co-seismic and rainfall-triggered landslide pixels, for landslide conditioning factors: **a** slope angle, **b** slope position, **c** proximity to active faults, **d** distance from streams, **e** geological formations, and **f** slope aspect. Slope Aspect N: North, NE: Northeast, E: East, SE: Southeast, S: South, SW: Southwest, W: West, and NW: Northwest; Geological formation G1: Precambrian dominantly granulites and gneisses, G2: Tertiary-Quaternary unconsolidated sedimentary, G3: Volcanic, G4: Surface water, G5: Precambrian dominantly metasedimentary, G6: Palaeozoic-Mesozoic sedimentary, G7: Precambrian metavolcanics, G8: Precambrian granites, and G9: Aswa Shear Zone. The dotted dashed black lines denote a target landslide frequency ratio of 1

6.1.2 Landslide conditioning factors

The distribution of landslide frequency ratios and the normalised overall relative land-slide areas corresponding to the most relevant landslide conditioning factors described in Sect. 5.2 are presented in Fig. 11a-f. In general, there is a significant contribution of co-seismic landslide pixels to the overall landslide hazard. For each landslide conditioning parameter, the normalised relative areas show the dominant landslide regions.

6.2 Comparison of landslide frequency ratios

Landslide frequency ratios covering the upper Manafwa catchment, stretching across Bududa district in Eastern Uganda, are compared with the findings of Nakileza and Nedala (2020) who characterized the morphometric conditions underpinning the spatial and temporal dynamics of landslide hazards along the volcanics of Mount Elgon following the study by Bamutaze (2019). The comparison based on slope angle (shown in Fig. 12a) indicates that except for slope angles less than 5°, the present study generally estimates approximately 10–60% higher landslide frequency ratios across all gradients. Although both studies utilised similar elevation models at 30 m resolution, the differences can be attributed to the fact that whilst Nakileza and Nedala (2020) assessed only rainfall-triggered landslides, the present work integrates both co-seismic and rainfall-induced landslide pixels to assess landslide frequency ratios. Moreover, landslide scars previously reported in Namisindwa and Bududa (DesInventar 2020) are included herein. Furthermore, Fig. 12b shows that the landslide frequency ratios for slope aspect estimated in the present study agree well with the predictions of Nakileza and Nedala (2020); further indicating that co-seismic events are not substantially affected by slope aspect.

On the other hand, the spatial distribution of landslide scars and the isoseismals of the two scenario earthquakes which extensively triggered landslides in Bundibugyo, Kasese, Bunyangabu, Kabarole and Ntoroko districts of western Uganda is mapped in Fig. 13a. It is seen that majority of landslides occurred along the active fault segments located in Bundibugyo and Kasese. Moreover, many medium-size landslides mapped within 2 km of active faults were possibly triggered by earthquakes in the region. Landslide frequency ratios derived from both rainfall-triggered and earthquake-induced landslide pixels are compared with frequency ratios determined by considering co-seismic landslide pixels only.
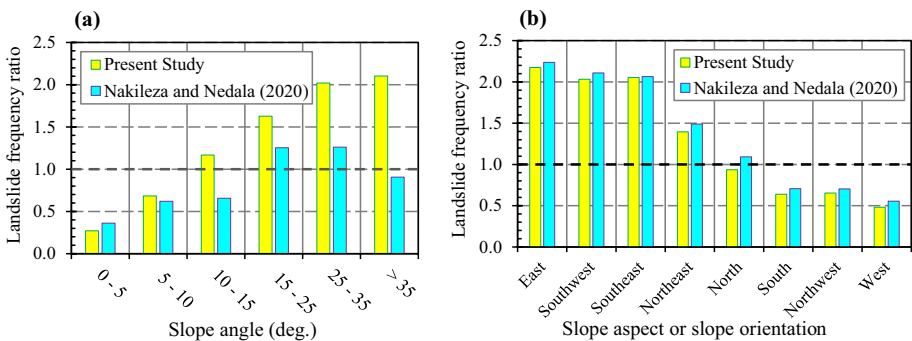

Fig. 12 Overall landslide frequency ratios covering the upper Manafwa catchment across Bududa district compared with the study by Nakileza and Nedala (2020), derived for: **a** slope angle, **b** slope aspect
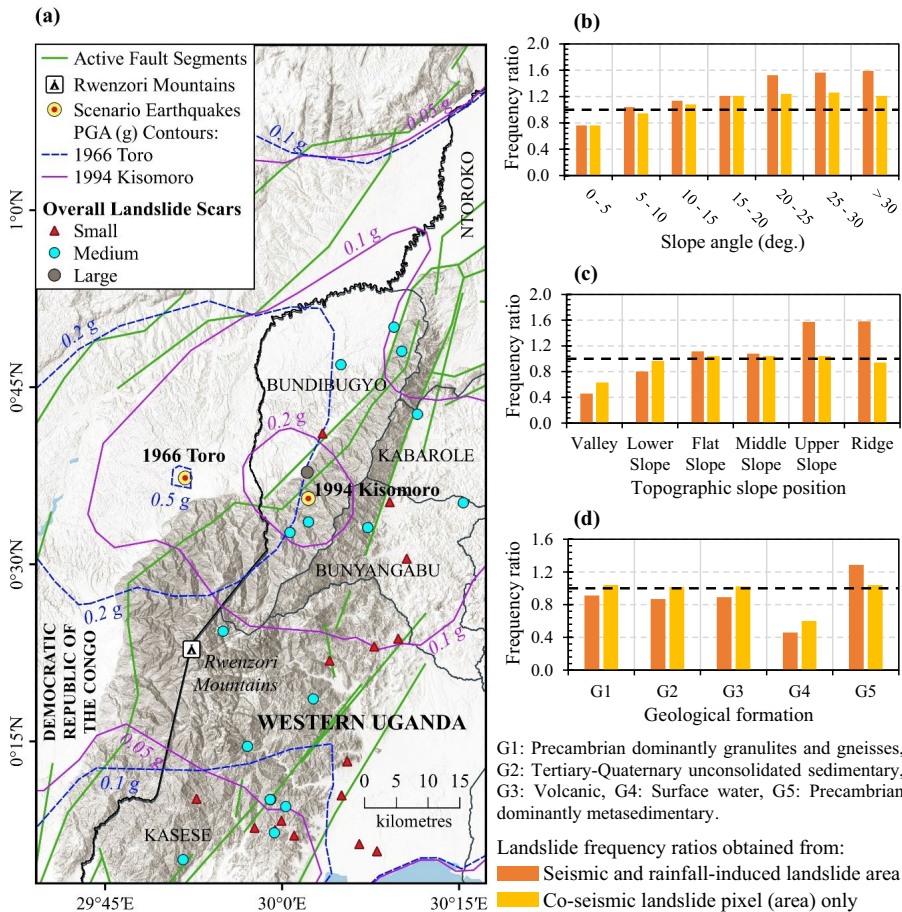
Fig. 13 a Spatial distribution of landslide scars and epicentres of scenario earthquakes which triggered landslides in western Uganda; and comparison of the overall and co-seismic landslide frequency ratios for selected landslide conditioning parameters: **b** slope angle, **c** slope position, and **d** geology

The landslide frequency ratios corresponding to slope angles and slope position (Fig. 13b-c) indicate that co-seismic landslide pixels contribute significantly to the overall landslide hazard in these regions. As further indicated in Fig. 13d, Precambrian dominantly granulites and gneisses, Volcanic and Tertiary-Quaternary unconsolidated sedimentary geological formations are predominantly more susceptible to earthquake-triggered landslides.

6.3 Fuzzy membership and aggregation

Using the coefficient of determination method, fuzzy membership curves are fitted to the normalized frequency ratios for the scenario earthquakes and their average fuzzy memberships determined, as presented in Fig. 14a-b. In both cases, fuzzy *MS Large* (sigmoid shape defined by mean and standard deviation) transformation function in which large values are more likely to be a member of the fuzzy set is used. In order to better represent the inferred
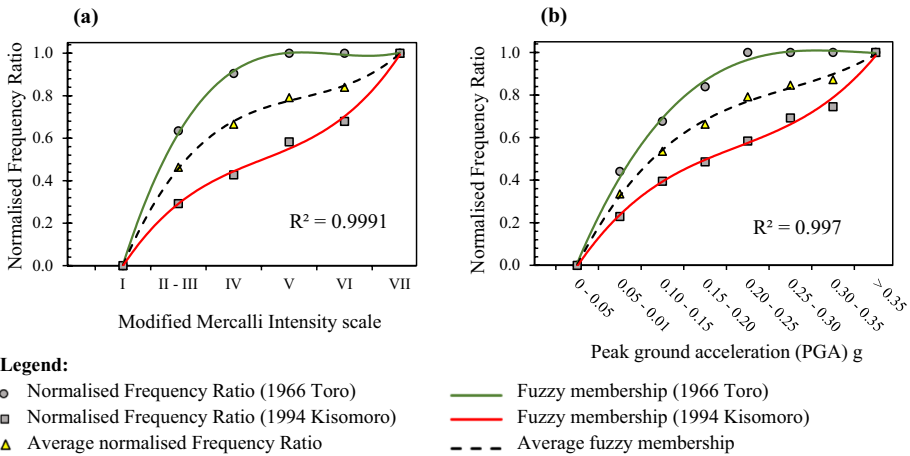
(a)

(b)

Modified Mercalli Intensity scale

Peak ground acceleration (PGA) g

Legend:

- ○ Normalised Frequency Ratio (1966 Toro)
- □ Normalised Frequency Ratio (1994 Kisomoro)
- △ Average normalised Frequency Ratio

— Fuzzy membership (1966 Toro)

— Fuzzy membership (1994 Kisomoro)

- - - Average fuzzy membership

Fig. 14 Normalized landslide frequency ratios and fuzzy curves for the 1966 Toro and 1994 Kisomoro earthquakes; assessed in terms of: **a** MMI scale, and **b** PGA on Type A rock/soil condition

influence of co-seismic factors and to account for any data inconsistencies, the fuzzy membership curve for the 1966 Toro earthquake is further subjectively adjusted from semi-data driven best fit curves so as to meaningfully represent larger memberships for higher PGA classes.

Using the suitable fuzzy membership functions, fuzzy membership maps describing the relative influence of landslide conditioning parameters on a 0–1 scale (0 represents low hazard and 1 denotes high hazard susceptibility) are derived from the distribution of landslide frequency ratios and mapped in Fig. 15a-c. In addition, the seismic hazard map on reference rock site conditions derived in terms of PGA (g) for a 475-year return period (presented in Fig. 6a) is similarly normalised as shown in Fig. 15d.

6.4 Relative probability of co-seismic landslide in western Uganda

Using the fuzzy *GAMMA* overlay tool ($\gamma = 0.95$) of *ArcGIS* (Raines et al. 2010), the fuzzy membership map corresponding to each landslide conditioning factor is individually correlated with normalised landslide frequency ratio-based PGA values corresponding to a 475-year return period on reference rock site conditions (Fig. 15d) in order to map the relative probability of co-seismic landslide hazard for each pixel. Since earthquake-induced landslides are typically concentrated in the Kigezi and Rwenzori sub-regions, and to more meaningfully depict the relative probability of co-seismic landslide hazard, the susceptibility maps shown in Fig. 16a-f are derived for the western part of the country only.

6.5 Co-seismic and rainfall-induced landslide susceptibility maps

The relative co-seismic landslide hazard susceptibility maps for Uganda shown in Fig. 17a-b are respectively derived by executing the GIS-based fuzzy *SUM* (Eq. 4) and fuzzy *PRODUCT* (Eq. 5) overlay tools. Whilst the landslide hazard susceptibility map based on fuzzy *SUM* (Fig. 17a) shows a wider distribution of co-seismic landslides, the map derived following
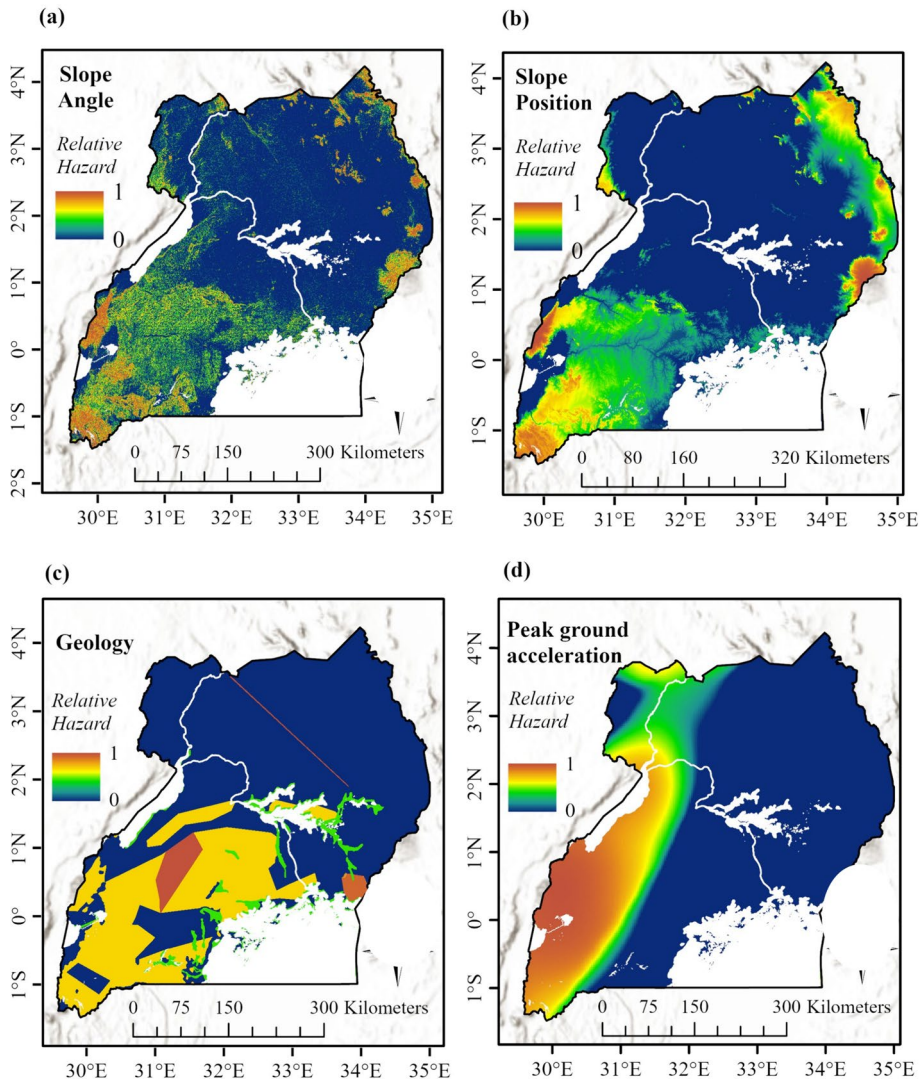
Fig. 15 Fuzzy membership maps for selected landslide conditioning factors: **a** slope angle, **b** slope position, **c** geology, and **d** landslide frequency ratio-based PGA (g) for a 475-year return period

fuzzy *PRODUCT* (Fig. 17b) indicates that co-seismic landslides are mainly concentrated in western Uganda. In addition, the GIS-based fuzzy *GAMMA* (Eq. 6) overlay tool (with $\gamma = 0.95$) is used to generate the relative co-seismic and rainfall-triggered landslide hazard susceptibility maps shown in Fig. 18a-b, respectively.
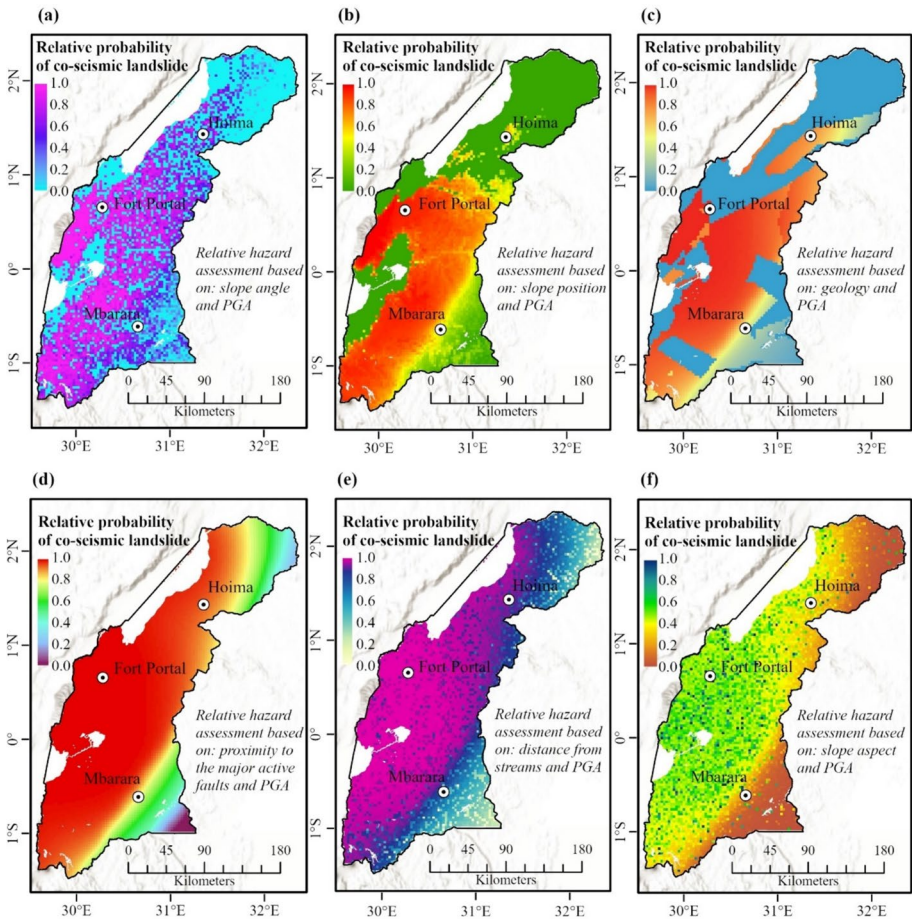
Fig. 16 Relative probability of co-seismic landslides in western Uganda, based on the conditioning factors and normalised landslide frequency ratio-based earthquake hazard map derived in terms of PGA (g) for a 475-year return period and overlaid for: **a** slope angle, **b** topographic slope position, **c** geology, **d** proximity to major active faults, **e** distance from streams, and **f** slope aspect

7 Validation of landslide susceptibility maps

The accuracy of landslide susceptibility maps proposed in this work is validated using the area under the receiver operating characteristic curve method in which success rate curves show the model performance (Chung and Fabbri 1999; Frattini et al. 2010; van Westen et al. 2003a). To verify whether the fuzzy overlay operators described in Eqs. (2–6) accurately predict the occurrence or non-occurrence of pre-established (known) landslide scars, the trade-off between false-positive and false-negative rates are graphically represented using the receiver operating characteristic (ROC) curves prior to determining area under curve (AUC) values (Gupta et al. 2023). False-positive rate λ_{FP} and true-positive rate λ_{TP} are defined as follows:
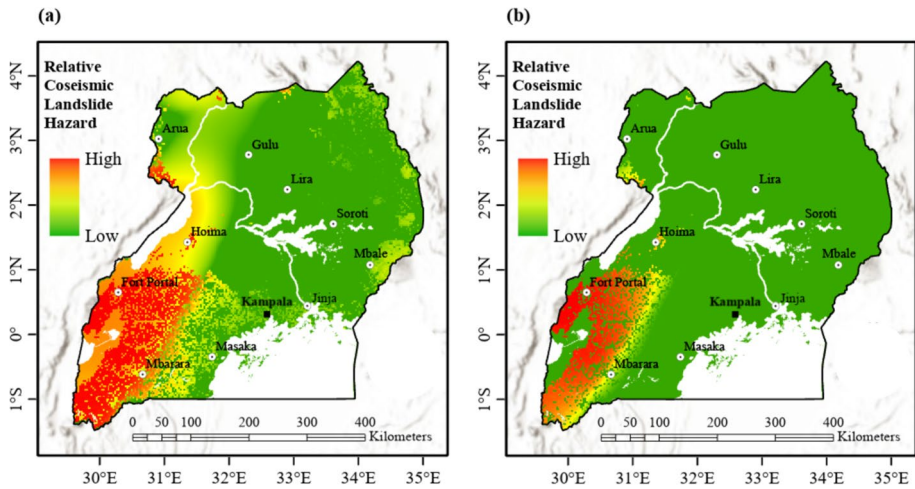
Fig. 17 Overall relative co-seismic landslide hazard susceptibility maps of Uganda obtained by combining landslide conditioning factors and normalised landslide frequency ratio-based PGA values, generated using the GIS-based fuzzy overlay tool: **a** Fuzzy *SUM* and **b** Fuzzy *PRODUCT*
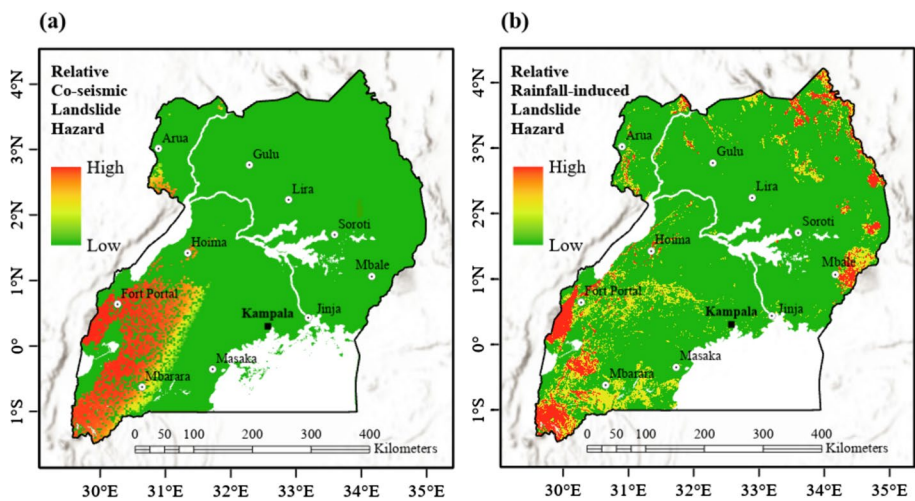

Fig. 18 **a** Relative co-seismic landslide hazard susceptibility based on various landslide conditioning factors and normalised frequency ratio-based PGA (g), and **b** Relative landslide hazard susceptibility obtained for conditioning parameters responsible for rainfall-induced landslides only. Both maps are generated using the GIS-based fuzzy GAMMA overlay tool with γ = 0.95

$$\lambda_{FP} = 1 - \frac{TN}{TN + FP} \tag{8}$$

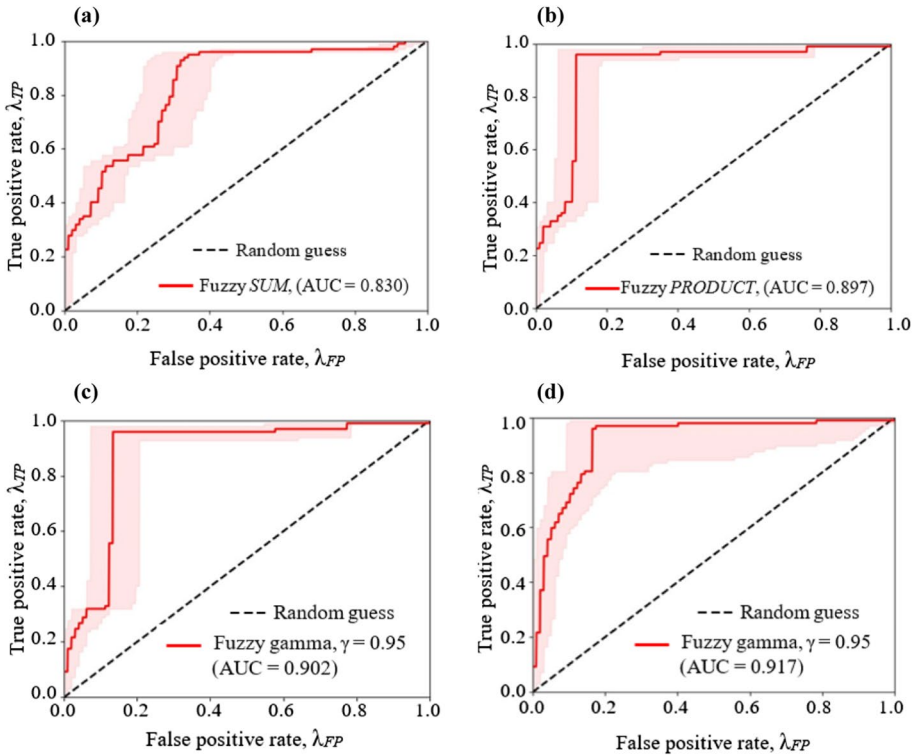$$\lambda_{TP} = \frac{TP}{TP + FN} \tag{9}$$

Fig. 19 Variation of true and false positive rates (AUC-ROC values) used to validate relative landslide hazard susceptibility maps derived for: **a** co-seismic fuzzy *SUM*, **b** co-seismic fuzzy *PRODUCT*, **c** co-seismic fuzzy *GAMMA* with γ = 0.95, and **d** rainfall-induced fuzzy *GAMMA* with γ = 0.95

where *TN* (true negative) and *TP* (true positive) represent the count of correctly grouped pixels, *FN* (false negative) and *FP* (false positive) indicate the count of erroneously categorised pixels. Herein, landslide pixels are binned into 100 equal intervals and the number of landslide scars in each interval is summed (Miles and Keefer 2009). By comparing the proportion of total landslides to the proportion of predictive bins in which landslide scars are mapped from highest to lowest (Beguería 2006; Pradhan and Lee 2010; Sema et al. 2017), the accuracy or success rate of the predictive models is assessed. In this work, success rate or model performance is defined by the AUC (ranging between 0.5 and 1.0) from which the highest value indicates the optimal approach (Nandi and Shakoor 2010). Whereas an AUC value equal to 1.0 represents a perfect forecast or prediction, AUC ≤ 0.5 implies that the model does not predict landslide occurrences any better than any random guess (Gupta et al. 2023). In general, AUC values exceeding 0.7 are a good representation and deem the model to be successful (Kritikos et al. 2015).

Success rates of landslide susceptibility maps shown in Fig. 17a-b, obtained using fuzzy *SUM* and fuzzy *PRODUCT*, are indicated in Fig. 19a-b. The landslide susceptibility map derived from fuzzy *PRODUCT* (Fig. 17b) indicates a success rate of 89.7% (Fig. 19b) and is more accurate compared with the 83.0% (Fig. 19a) performance level obtained from fuzzy *SUM* map shown in Fig. 17a. Although the performance levels obtained using fuzzy *SUM* and fuzzy *PRODUCT* may be deemed successful (AUC > 0.7), more accurate
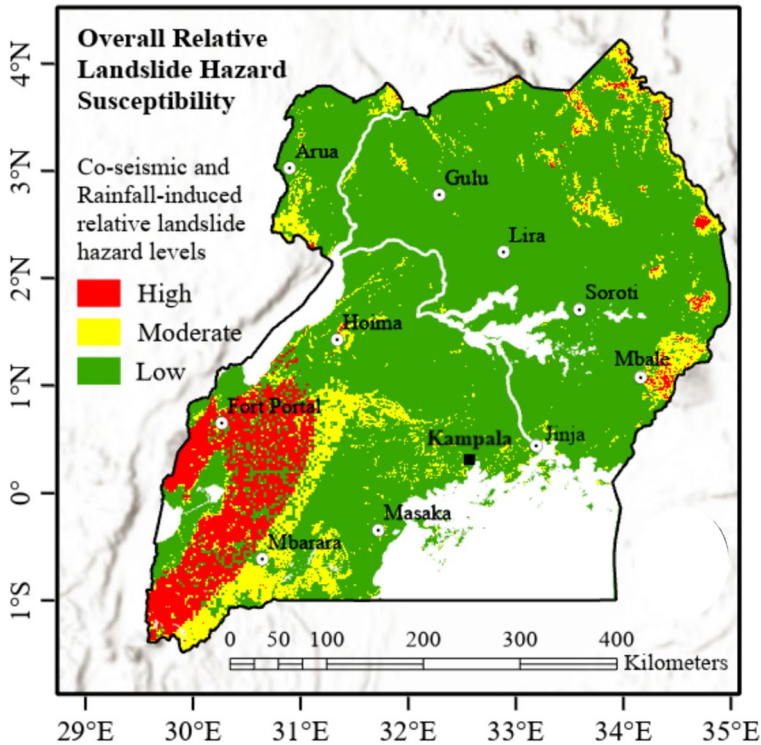
Fig. 20 Overall relative landslide hazard susceptibility map of Uganda combining both co-seismic and rainfall conditioning factors

predictions are obtained by implementing fuzzy *GAMMA* (Kritikos et al. 2015). The effect of γ-value on landslide susceptibility maps is assessed by generating AUC for various models in which γ is set between 0.65 and 0.95 in a 0.1 interval. As depicted in Fig. 19c, an optimal model performance level of 90.2% is obtained for co-seismic landslide susceptibility map in which γ is set to 0.95 (Fig. 18a). Following the relative landslide susceptibility map based on topographic factors responsible for rainfall-induced landslides (Fig. 18b), the evaluation of AUC indicates a higher success rate of 91.7% as shown in Fig. 19d. The improved success rate can be attributed to the accurate DEM from which landslide conditioning factors are modelled.

8 Final landslide hazard susceptibility map

Subsequent to the relative co-seismic and rainfall-induced landslide hazard susceptibility maps shown in Fig. 18a-b, the final overall relative landslide hazard map combining co-seismic and rainfall conditioning parameters is as shown in Fig. 20. As expected, whereas several parts of Uganda are susceptible to low landslide hazard, majority of the country's highlands and seismically active zones (e.g., Fort Portal city) are prone to moderate and high intensities of slope failures. For the purpose of detailed absolute landslide hazard assessments envisaged as a possible extension of the present study, the overall landslide

Table 2 Critical landslide conditions under which detailed landslide hazard assessments are highly recommended for buildings and infrastructure developments

Landslide parameters	Minimum conditions
Peak ground acceleration	Considering a 10% POE in 50 years (475-year return period), PGA on reference rock site conditions ≥ 0.1 g
Geology	Highly weathered outcropping rocks of Precambrian granites (G8), Precambrian dominantly granulites and gneisses (G1), and Precambrian dominantly metasedimentary (G5) geological structure
Slope position	TPI ≥ 3.8, which categorises all slope categories except U-shaped valley or spread water, and deeply incised streams valleys
Slope angle	≥ 10 degrees
Proximity to active faults	≤ 40 km
Distance from streams	≤ 1.25 km

zones are broadly categorised into three hazard levels of low, moderate, and high; respectively depicted as *green*, *yellow*, and *red* pixels. Based on the findings of this work, critical landslide conditions under which detailed absolute landslide hazard assessments are highly recommended for buildings and infrastructure developments are summarised in Table 2.

Although detailed assessments may be neglected in low (*green*) hazard zones, this study recommends mandatory analysis in high (*red*) landslide hazard areas. On the other hand, prior to construction and infrastructure developments within moderate (*yellow*) hazard regions, it is recommended that detailed landslide hazard analysis be conducted if the following critical conditions presented in Table 2 are satisfied. Detailed landslide hazard analysis is encouraged in regions of moderate landslide hazard level comprising highly weathered outcropping rocks of Precambrian granites, dominantly metasedimentary, and granulites and gneisses geologies within 80 km from major active faults; where the bedrock PGA ≥ 0.1 g over a 475-year return period, topographic position index ≥ 3.8, slope gradient ≥ 10 degrees, and the distance from streams ≤ 1.25 km.

As an initial step, a local planning and regulatory approach that aims to manage development within disaster-prone areas, adopt and enforce robust building codes, advocate for good environmental practices like restoration of vegetation cover and afforestation, resettlement plans and utilization of disaster-prone areas for specific seasonal activities should be applied and appropriately implemented. Further to natural system protection remedies and raising community awareness, infrastructure protection and structural retrofitting, removal of existing constructions from disaster-prone areas, structural mitigation techniques and protection of critical facilities like hospitals should be applied.

9 Discussion

In this work, a detailed co-seismic and rainfall-triggered landslide hazard susceptibility assessment is performed for Uganda using a geospatial-based fuzzy logic approach and the findings largely confirm that several parts of the country are prone to slope failures of varying degrees. To begin with the assessment of landslide frequency ratios, Fig. 10b shows that for the 1966 Toro earthquake, landslide frequency ratios increase to a maximum value of 2.24 at PGA values ranging between 0.20 and 0.25 g, beyond which the likelihood of landslide occurrence reduces. On the other hand, a maximum landslide

frequency ratio of 2.25 is estimated for PGA raising to 0.35 g for the 1994 Kisomoro earthquake. The main mechanical reason behind this trend is that shear resistance of the exposed material is more likely to be exceeded when higher stresses are induced by stronger shaking intensity, thereby inducing landslides of even larger magnitudes (Towhata et al. 2022; Valagussa et al. 2019).

Following the determination of landslide frequency ratios shown in Fig. 11a, it is seen that although majority of Uganda's territory is largely dominated by slope angles between 0 and 5°, there is a significant contribution of rainfall-induced landslides from which frequency ratios increase with increasing slopes of up to 50°. Except for slopes < 5°, co-seismic landslide frequency ratios across slope classes range between 1.43 and 2.67; implying that earthquakes are capable of triggering co-seismic landslides along most slopes as indicated by Valagussa et al. (2019). Whereas the instability of lower slopes covered with thick residual soils is largely initiated by a high water table (Zhuang et al. 2015), overall landslide frequency ratios increase with slope angles increasing to a maximum of 40°. The increase is partly driven by gravitational forces from which greater shear stresses are generated along steeper slopes (Silalahi et al. 2019; Torizin 2011). However, the decline in landslide frequency ratios for slopes > 40° is partially attributed to increased shear resistance of the rock mass where relative landslide areas are minimal. The result presented in Fig. 11a is consistent with the findings of Bizimana and Sönmez (2015) which indicate that landslide-prone areas are situated along concave slope angles exceeding 41°. In contrast, Bamutaze (2019) reported the highest frequency ratio along slopes of up to 31° in Elgon region while Nseka et al. (2019) indicated maximum frequency ratios for gradients of 25–35° in western Uganda. However, the analyses by Nseka et al. (2019) and Bamutaze (2019) ignored co-seismic landslides and did not cover the entire country.

Owing to the topographic variations induced by soil creep, incised channels, spurs, and ridges, the assessment of topographic slope position shown in Fig. 11b indicates the highest overall landslide frequency ratios along upper slopes, followed by ridges and middle slopes; with the major contribution of rainfall-induced landslides expected along these slope positions. Except for lower slopes, there is a strong correlation between co-seismic landslides and the other slope positions. Due to localised escalation of ground motion amplitudes generated by the propagation of seismic waves (Meunier et al. 2008), the trend shown in Fig. 11b is partly attributed to greater seismic amplification along ridgelines which in turn increases the likelihood of slope failures (Buech et al. 2010). Moreover, the lateral spread of seismic waves propagating along river banks within valleys can significantly increase the likelihood of co-seismic landslide.

On the other hand, the highest landslide frequency ratios and relative landslide areas are observed within 40 km from fault traces as seen in Fig. 11c. As expected, regions closer to active faults are more susceptible to co-seismic landslides since previous earthquakes induce various weakening mechanisms which subsequently cause reduction in the strength of the neighbouring rock mass (Kellogg 2001; Korup 2004). With regard to hydrology, assessed in terms of distance from streams as shown in Fig. 11d, stream banks located within 0.75 km (comprising the majority of relative landslide areas) are overall more vulnerable to landslides. This is because fluvial erosion along streams causes higher shearing stresses. Moreover, the collective reduction in shear strength of slope materials located near streams, caused by presence of soil moisture and increased pore water pressure, is an exacerbating factor (Berhane et al. 2023; Korup 2004; Kritikos et al. 2015). While many rainfall-induced landslides may be triggered at ≤ 1.25 km, most co-seismic landslides are within 1.00 km from streams.

Regarding the variation of landslide frequency ratio and relative landslide areas with geology, Precambrian dominantly Metasedimentary and Precambrian granites (outcropping rocks which include a certain degree of fracturing and weathering) exhibit the highest overall landslide frequency ratios as shown in Fig. 11e. Within Uganda's Precambrian basement/craton, the Precambrian dominantly metasedimentary, and Precambrian dominantly granulites and gneisses geologies are exposed to relatively high likelihood of co-seismic landslides. Gneisses geologies comprise coarse to medium grained banded metamorphic rocks (rich in feldspars and quartz, and mica and aluminous/ferromagnesian silicates) which are formed from igneous or sedimentary rocks. The correlation of landslides with the associated geologies is attributed to the reduction in material strengths as water percolates through columnar joints existing along geological fissures. Although the assessment of slope aspect (Fig. 11f) shows uniform landslide distribution, the strongest correlation exists in the eastern aspect. This can be attributed to moisture and the flow direction of storm water runoff, essentially influenced by the direction of sunlight (Berhane et al. 2023).

The relative earthquake-triggered landslide hazard susceptibility map shown in Fig. 18a shows that only western Uganda is exposed to the highest level partly due to its active seismicity and geo-tectonic environment. Although the worst hazard level is predicted around the Rwenzori and Kigezi sub-regions, Uganda's north-western boarder (near Arua city) and Albertine graben (around Hoima city) can expect some co-seismic landslides. On the other hand, the relative rainfall-triggered landslide hazard susceptibility map shown in Fig. 18b (obtained for conditioning factors only, without considering earthquake characteristics) confirms that several highlands are prone to rainfall-triggered landslides. In this regard, Uganda's directorate of disaster preparedness and management under office of the Prime Minister should develop suitable disaster risk mitigation measures aimed at reducing future earthquake and landslide risks across Uganda. The findings of this work can be used to systematically suggest pre- and post-disaster remedies and inform the implementation of landslide prevention and mitigation strategies outlined in the country's national policy for disaster preparedness and management (NPDPM 2010). The major limitation of this study is the lack of detailed information relating to co-seismic landslide occurrences and this points to the urgent need for a more robust scheme of monitoring, recording and mapping landslides, especially in the potentially hazardous sites.

10 Conclusions

This study demonstrates the ability of a fuzzy logic approach combined with geospatial techniques in the development of a comprehensive national co-seismic and rainfall-induced landslide hazard susceptibility assessment, despite scarce historical landslide inventories. Topographical maps, geological maps, 30-m digital elevation models and co-seismic and rainfall-induced landslide pixel datasets are collected from available resources. Five landslide conditioning factors including slope angle, topographic slope position, distance from streams, proximity to major active faults and geology are identified as the most prevalent conditioning factors. A statistical bivariate method is used to calculate the spatial relationship between landslide conditioning factors and their locations prior to implementation of fuzzy membership functions and subsequent fuzzy maps. The average fuzzy memberships, obtained for the 1966 Toro and 1994 Kisomoro earthquakes, is assigned to the seismic hazard map produced for a 475-year return period on reference rock site conditions. Landslide

conditioning factor maps are quantified, aggregated with the fuzzy membership-based PGA and their spatial distribution overlaid to derive final fuzzy maps showing relative co-seismic and rainfall-triggered landslide hazards. The results show that areas of Precambrian granites located in ridges and upper slope gradients between 35 and 40° have the highest landslide hazard susceptibility. The findings conclude that Kigezi and Rwenzori sub-regions in western Uganda are highly prone to co-seismic landslides while landslide occurrences across the other parts are largely driven by rainfall. This work offers valuable insights into the relative co-seismic landslide hazard susceptibility towards informing the ministry of relief, disaster preparedness and management on the application of suitable landslide risk reduction strategies. As a precursor, the relevant government ministries and agencies should apply concerted efforts to strengthen existing pre- and post-disaster mitigation strategies aimed and reducing losses due to landslides in Uganda.

Declarations

References

Ahmed B (2015) Landslide susceptibility mapping using multi-criteria evaluation techniques in Chittagong Metropolitan Area. Bangladesh Landslides 12(6):1077–1095

Akera S (2012) Towards implementation of the Uganda National Disaster Preparedness and Management Policy. ISDR, Disaster risk reduction in Africa. Special issue on drought

Aleotti P, Chowdhury R (1999) Landslide hazard assessment: summary review and new perspectives. Bull Eng Geol Environ 58(1):21–44

Aleotti P, Baldelli P, Polloni G, Puma F (1998) Keynote paper: different approaches to landslide hazard assessment. In: Proceedings of the second conf environ management (ICEM-2)

Anbalagan R, Singh B (1996) Landslide hazard and risk assessment mapping of mountainous terrains—a case study from Kumaun Himalaya, India. Eng Geol 43(4):237–246

Anbalagan R, Kumar R, Lakshmanan K, Parida S, Neethu S (2015) Landslide hazard zonation mapping using frequency ratio and fuzzy logic approach, a case study of Lachung Valley, Sikkim. Geoenviron Disasters 2:1–17

Athanasopoulos G, Pelekis P, Leonidou E (1999) Effects of surface topography on seismic ground response in the Egion (Greece) 15 June 1995 earthquake. Soil Dyn Earthq Eng 18(2):135–149

Ayalew L, Yamagishi H (2005) The application of GIS-based logistic regression for landslide susceptibility mapping in the Kakuda-Yahiko Mountains, Central Japan. Geomorphol 65(1–2):15–31

Baeza C, Corominas J (1996) Assessment of shallow landslide susceptibility by means of statistical techniques. Landslides

Baker J, Bradley B, Stafford P (2021) Seismic hazard and risk analysis. Cambridge University Press

Bamutaze Y (2019) Morphometric conditions underpinning the spatial and temporal dynamics of landslide hazards on the volcanics of Mt. Elgon, Eastern Uganda. In Emerging Voices in Natural Hazards Research (pp 57–81). Elsevier

Bathrellos GD, Skilodimou HD, Zygouri V, Koukouvelas IK (2021) Landslide: a recurrent phenomenon? Landslide hazard assessment in mountainous areas of central Greece. Z Geomorphol 63:95–114

Bauer F, Karl M, Glasmacher U, Nagudi B, Schumann A, Mroszewski L (2012) The rwenzori mountains of western uganda-aspects on the evolution of their remarkable morphology within the albertine rift. J Afr Earth Sci 73:44–56

Beguería S (2006) Validation and evaluation of predictive models in hazard assessment and risk management. Nat Hazards 37:315–329

Berhane G, Gebrehiwot A, Abay A (2023) Landslide susceptibility mapping in the Adwa Volcanic Mountain Plugs, Northern Ethiopia: a comparative analysis of frequency ratio and analytical hierarchy process methods. Geomat Nat Hazards Risk 14(1):2281244

Bizimana H, Sönmez O (2015) Landslide occurrences in the hilly areas of Rwanda, their causes and protection measures. Dis Sci Eng 1(1):1–7

Bonham-Carter GF (1994) Geographic information systems for geoscientists: modelling with GIS. Elsevier

Bortolami G, De Luca D, Masciocco L (1994) Studio sulla realizzazione di carte della franosità a scala regionale. In Atti del IV Convegno Internazionale di Geoingegneria Difesa e Valorizzazione del Suolo e degli Acquiferi (Vol 1, pp 21–27). Associazione Mineraria Subalpina

Bourenane H, Bouhadad Y, Guettouche MS, Braham M (2015) GIS-based landslide susceptibility zonation using bivariate statistical and expert approaches in the city of Constantine (Northeast Algeria). Bull Eng Geol Environ 74(2):337–355

Broeckx J, Maertens M, Isabirye M, Vanmaercke M, Namazzi B, Deckers J, Tamale J, Jacobs L, Thiery W, Kervyn M (2019) Landslide susceptibility and mobilization rates in the Mount Elgon region, Uganda. Landslides 16(3):571–584

Brune JN (2001) Shattered rock and precarious rock evidence for strong asymmetry in ground motions during thrust faulting. Bull Seismol Soc Am 91(3):441–447

Buech F, Davies T, Pettinga J (2010) The little red hill seismic experimental study: topographic effects on ground motion at a bedrock-dominated mountain edifice. Bull Seismol Soc Am 100(5A):2219–2229

Bufalini M, Materazzi M, De Amicis M, Pambianchi G (2021) From traditional to modern 'full coverage'geomorphological mapping: a study case in the Chienti river basin (Marche region, central Italy). J Maps 17(3):17–28

Bughi S, Aleotti P, Bruschi R, Andrei G, Milani G, Scarpelli G, Sakellariadi E (1996) Slow movements of slopes interfering with pipelines: modeling and monitoring

Caniani D, Pascale S, Sdao F, Sole A (2008) Neural networks and landslide susceptibility: a case study of the urban area of Potenza. Nat Hazards 45(1):55–72

Capitani M, Ribolini A, Bini M (2013) The slope aspect: a predisposing factor for landsliding? CR Geosci 345(11–12):427–438

Carrara A (1983) Multivariate models for landslide hazard evaluation. J Int Assoc Math Geol 15:403–426

Carrara A, Merenda L (1976) Landslide inventory in northern Calabria, southern Italy. Geol Soc Am Bull 87(8):1153–1162

Carrara A, Cardinali M, Guzzetti F (1992) Uncertainty in assessing landslide hazard and risk. ITC J 2:172–183

Cellek S (2021) The effect of aspect on landslide and its relationship with other parameters. In Landslides. IntechOpen

Choubey V, Chaudhari S, Litoria P (1992) Landslide hazard zonation in Uttarkashi and Tehri districts, UP Himalaya. International symposium on landslides, India

Chousianitis K, Del Gaudio V, Sabatakakis N, Kavoura K, Drakatos G, Bathrellos GD, Skilodimou HD (2016) Assessment of earthquake-induced landslide hazard in Greece: From Arias intensity to spatial distribution of slope resistance demand. Bull Seismol Soc Am 106(1):174–188

Chowdhury R, Bertoldi C (1977) Residual shear tests on soil from two natural slopes

Chowdhury R (1984) Recent developments in landslide studies: probabilistic methods-state-of-art-report. Proceedings of the 4th international symposium on landslides

Chung CJF, Fabbri AG (1999) Probabilistic prediction models for landslide hazard mapping. Photogramm Eng Remote Sens 65(12):1389–1399

Clerici A, Dall'Olio N (1995) La realizzazione di una Carta della stabilità potenziale dei versanti mediante tecniche di Analisi Statistica Multivariata e un Sistema d'Informazione Geografica. Rep Inst Hydrol 4:49–57

Dahal RK, Hasegawa S, Yamanaka M, Dhakal S, Bhandary NP, Yatabe R (2009) Comparative analysis of contributing parameters for rainfall-triggered landslides in the Lesser Himalaya of Nepal. Environ Geol 58(3):567–586

Dai F, Xu C, Yao X, Xu L, Tu X, Gong Q (2011) Spatial distribution of landslides triggered by the 2008 Ms 8.0 Wenchuan earthquake China. J Asian Earth Sci 40(4):883–895

Davis LL, West LR (1973) Observed effects of topography on ground motion. Bull Seismol Soc Am 63(1):283–298

DesInventar (2020) The national disaster loss database https://www.desinventar.net/DesInventar/profiletab.jsp (accessed 24.08.2022)

Donati L, Turrini M (2002) An objective method to rank the importance of the factors predisposing to landslides with the GIS methodology: application to an area of the Apennines (Valnerina; Perugia, Italy). Eng Geol 63(3–4):277–289

Doocy S, Russell E, Gorokhovich Y, Kirsch T (2013) Disaster preparedness and humanitarian response in flood and landslide-affected communities in Eastern Uganda. Dis Prev Manag 22(4):326–339

Drăguţ L, Blaschke T (2006) Automated classification of landform elements using object-based image analysis. Geomorphology 81(3–4):330–344

Dramis F, Sorriso-Valvo M (1994) Deep-seated gravitational slope deformations, related landslides and tectonics. Eng Geol 38(3–4):231–243

Dubois D, Prade H (1985) A review of fuzzy set aggregation connectives. Inf Sci 36(1–2):85–121

Eggermont H, Damme KV, Russell JM (2009) Rwenzori mountains (mountains of the moon): headwaters of the white Nile. In: The Nile (pp 243–261). Springer, Cham

Fairhead J, Stuart G (1982) The seismicity of the East African rift system and comparison with other continental rifts. Contin Oceanic Rifts 8:41–61

Fenti V, Silvano S, Spagna V (1979) Methodological proposal for an engineering geomorphological map Forecasting rockfalls in the alps. Bull Eng Geol Environ 19(1):1

Frattini P, Crosta G, Carrara A (2010) Techniques for evaluating the performance of landslide susceptibility models. Eng Geol 111(1–4):62–72

Furman T, Kaleta KM, Bryce JG, Hanan BB (2006) Tertiary mafic lavas of Turkana, Kenya: constraints on East African plume structure and the occurrence of high-μ volcanism in Africa. J Petrol 47(6):1221–1244

Gorsevski PV, Gessler PE, Jankowski P (2003) Integrating a fuzzy k-means classification and a Bayesian approach for spatial prediction of landslide hazard. J Geogr Syst 5(3):223–251

Gupta P, Anbalagan R (1997) Slope stability of Tehri dam reservoir area, India, using landslide hazard zonation (LHZ) mapping. Q J Eng Geol Hydrogeol 30(1):27–36

Gupta RP, Kanungo DP, Arora MK, Sarkar S (2008) Approaches for comparative evaluation of raster GIS-based landslide susceptibility zonation maps. Int J Appl Earth Obs Geoinf 10(3):330–341

Gupta K, Satyam N, Gupta V (2023) Probabilistic assessment of seismically triggered landslide hazard for Uttarakhand (India) in the Western Himalayas. Nat Hazards 118(1):669–689

Hartlen J, Viberg L (1988) General report: evaluation of landslide hazard. Int Sympos Landslides 5

Havenith H-B, Vanini M, Jongmans D, Faccioli E (2003) Initiation of earthquake-induced slope failure: influence of topographical and other site specific amplification effects. J Seismol 7(3):397–412

He Y, Beighley RE (2008) GIS-based regional landslide susceptibility mapping: a case study in southern California. Earth Surf Process Landf J Br Geomorphol Res Group 33(3):380–393

Hearn G (1995) Landslide and erosion hazard mapping at Ok Tedi copper mine, Papua New Guinea. Q J Eng Geol Hydrogeol 28(1):47–60

Hervás J, Bobrowsky P (2009) Mapping: inventories, susceptibility, hazard and risk. Landslides Dis Risk Reduct 321–49:1

Ives JD, Messerli B (1981) Mountain hazards mapping in nepal introduction to an applied mountain research project. Mt Res Dev 1:223–230

Ives JD, Bovis MJ (1978) Natural hazards maps for land-use planning, San Juan Mountains, Colorado, USA*. Arct Alp Res 10(2):185–212

Jacobs L, Dewitte O, Poesen J, Delvaux D, Thiery W, Kervyn M (2016) The Rwenzori Mountains, a landslide-prone region? Landslides 13(3):519–536

Jacobs L, Dewitte O, Poesen J, Maes J, Mertens K, Sekajugo J, Kervyn M (2017) Landslide characteristics and spatial distribution in the Rwenzori Mountains, Uganda. J Afr Earth Sci 134:917–930

Jenness J, Brost B, Beier P (2013) Land facet corridor designer. USDA forest service rocky mountain research station

Jenness J (2006) Topographic position index (tpi_jen. avx_extension for Arcview 3. x, v. 1.3 a, Jenness Enterprises [EB/OL]

Jibson RW, Harp EL, Michael JA (2000) A method for producing digital probabilistic seismic landslide hazard maps. Eng Geol 58(3–4):271–289

Kanungo DP, Arora M, Sarkar S, Gupta R (2006) A comparative study of conventional, ANN black box, fuzzy and combined neural and fuzzy weighting procedures for landslide susceptibility zonation in Darjeeling Himalayas. Eng Geol 85(3–4):347–366

Kanungo D, Arora M, Sarkar S, Gupta R (2009) A fuzzy set based approach for integration of thematic maps for landslide susceptibility zonation. Georisk 3(1):30–43

Karp T, Scholz CA, McGlue MM (2012) Structure and stratigraphy of the Lake Albert Rift, East Africa: Observations from seismic reflection and gravity data

Karpouza M, Chousianitis K, Bathrellos GD, Skilodimou HD, Kaviris G, Antonarakou A (2021) Hazard zonation mapping of earthquake-induced secondary effects using spatial multi-criteria analysis. Nat Hazards 109:637–669

Kato S, Mutonyi R (2011) The challenges of managing increasing landslides vulnerability on mount Elgon ecosystem. Uganda: a case of human interactions with its environment on the verge of collapsing

Kayastha P (2012) Application of fuzzy logic approach for landslide susceptibility mapping in Garuwa sub-basin, East Nepal. Front Earth Sci 6(4):420–432

Kellogg KS (2001) Tectonic controls on a large landslide complex: Williams fork mountains near Dillon, Colorado. Geomorphology 41(4):355–368

Kienholz H (1978) Maps of geomorphology and natural hazards of grindelwald, Switzerland: scale 1: 10,000*. Arct Alp Res 10(2):169–184

Kingsbury P, Hastie W, Harrington A (1992) Regional landslip hazard assessment using a Geographic Information System. International symposium on landslides

Kitutu M, Muwanga A, Poesen J, Deckers JA (2009) Influence of soil properties on landslide occurrences in Bududa district, Eastern Uganda. Afr J Agric Res 4(7):611–620

Kitutu MG, Muwanga A, Poesen J, Deckers S (2011) Farmer's perception on landslide occurrences in Bududa District, Eastern Uganda. Afr J Agric Res 6(1):7–18

Knapen A, Kitutu MG, Poesen J, Breugelmans W, Deckers J, Muwanga A (2006) Landslides in a densely populated county at the footslopes of Mount Elgon (Uganda): characteristics and causal factors. Geomorphology 73(1–2):149–165

Koehn D, Lindenfeld M, Rümpker G, Aanyu K, Haines S, Passchier C, Sachau T (2010) Active transsection faults in rift transfer zones: evidence for complex stress fields and implications for crustal fragmentation processes in the western branch of the East African Rift. Int J Earth Sci 99:1633–1642

Korup O (2004) Geomorphic implications of fault zone weakening: slope instability along the Alpine Fault, South Westland to Fiordland. NZ J Geol Geophys 47(2):257–267

Kramer SL (1996) Geotechnical earthquake engineering. Pearson Education India

Kritikos T, Robinson TR, Davies TR (2015) Regional coseismic landslide hazard assessment without historical landslide inventories: a new approach. J Geophys Res Earth Surf 120(4):711–729

Larsen IJ, Montgomery DR (2012) Landslide erosion coupled to tectonics and river incision. Nat Geosci 5(7):468–473

Lee S, Pradhan B (2007) Landslide hazard mapping at Selangor, Malaysia using frequency ratio and logistic regression models. Landslides 4(1):33–41

Lee S, Sambath T (2006) Landslide susceptibility mapping in the Damrei Romel area, Cambodia using frequency ratio and logistic regression models. Environ Geol 50(6):847–855

Lee S, Talib JA (2005) Probabilistic landslide susceptibility and factor effect analysis. Environ Geol 47:982–990

Lee S-J, Komatitsch D, Huang B-S, Tromp J (2009) Effects of topography on seismic-wave propagation: An example from northern Taiwan. Bull Seismol Soc Am 99(1):314–325

Lees BG (1996) Neural network applications in the geosciences: an introduction. Comput Geosci 22(9):955–957

Leroi E (1996) Landslide hazard-risk maps at different scales: objectives, tools and developments. Landslides

Maasha N (1975) The seismicity and tectonics of Uganda. Tectonophysics 27(4):381–393

Marano KD, Wald DJ, Allen TI (2010) Global earthquake casualties due to secondary effects: a quantitative analysis for improving rapid loss analyses. Nat Hazards 52(2):319–328

Masaba S, Mungai DN, Isabirye M, Nsubuga H (2017) Implementation of landslide disaster risk reduction policy in Uganda. Int J Disaster Risk Reduct 24:326–331

Mavonga T (2007) Some characteristics of aftershock sequences of major earthquakes from 1994 to 2002 in the Kivu province, Western Rift Valley of Africa. Tectonophysics 439(1–4):1–12

McDougall I, Brown FH (2009) Timing of volcanism and evolution of the northern Kenya Rift. Geol Mag 146(1):34–47

Meherota G, Dharmaraju R, Kanungo D (1994) Landslide hazard zonation–a tool for environmental development and protection of hilly terrain. Man Mt 94:101–113

Meunier P, Hovius N, Haines JA (2008) Topographic site effects and the location of earthquake induced landslides. Earth Planet Sci Lett 275(3–4):221–232

Miles SB, Keefer DK (2009) Evaluation of CAMEL—comprehensive areal model of earthquake-induced landslides. Eng Geol 104(1–2):1–15

Mugagga F, Kakembo V, Buyinza M (2012) A characterisation of the physical properties of soil and the implications for landslide occurrence on the slopes of Mount Elgon, Eastern Uganda. Natl Hazards 60(3):1113–1131

Musinguzi M, Asiimwe I (2014) Application of geospatial tools for landslide hazard assessment for Uganda. S Afr J Geomat 3(3):302–314

Muwanga A, Schuman A, Biryabarema M (2001) Landslides in Uganda—documentation of a natural hazard. Documenta Naturae 136:111–115

Nagarajan R, Mukherjee A, Roy A, Khire M (1998) Technical note temporal remote sensing data and GIS application in landslide hazard zonation of part of Western Ghat, India

Nakileza BR, Nedala S (2020) Topographic influence on landslides characteristics and implication for risk management in upper Manafwa catchment, Mt Elgon Uganda. Geoenviron Disasters 7(1):1–13

Nandi A, Shakoor A (2010) A GIS-based landslide susceptibility evaluation using bivariate and multivariate statistical analyses. Eng Geol 110(1–2):11–20

NASA (2022) Rainfall-triggered landslides https://gpm.nasa.gov/applications/landslides (Accessed 20/07/2022)

Nefeslioglu HA, Gokceoglu C, Sonmez H, Gorum T (2011) Medium-scale hazard mapping for shallow landslide initiation: the Buyukkoy catchment area (Cayeli, Rize, Turkey). Landslides 8(4):459–483

Nguyen V, Chowdhury R (1984) Probabilistic analysis of mining spoil piles—two techniques compared. Int. J. Rock Mech. and Mining Sci., and Geomech. Abstr

NPDPM (2010) The National Policy for Disaster Preparedness and Management. Office of the Prime Minister

Nseka D, Kakembo V, Bamutaze Y, Mugagga F (2019) Analysis of topographic parameters underpinning landslide occurrence in Kigezi highlands of southwestern Uganda. Nat Hazards 99(2):973–989

Oleng M, Ozdemir Z, Pilakoutas K (2024) Probabilistic seismic hazard assessment framework for Uganda: a stochastic event-based modelling approach. Bull Earthq Eng. https://doi.org/10.1007/s10518-024-01856-6

Pachauri A, Pant M (1992) Landslide hazard mapping based on geological attributes. Eng Geol 32(1–2):81–100

Pagani M, Monelli D, Weatherill G, Danciu L, Crowley H, Silva V, Henshaw P, Butler L, Nastasi M, Panzeri L (2014) OpenQuake engine: an open hazard (and risk) software for the global earthquake model. Seismol Res Lett 85(3):692–702

Pagani M, Silva V, Rao A, Simionato M, Johnson K (2023) OpenQuake Engine Manual

Petley D (2012) Global patterns of loss of life from landslides. Geology 40(10):927–930

Pradhan B, Lee S (2010) Delineation of landslide hazard areas on Penang Island, Malaysia, by using frequency ratio, logistic regression, and artificial neural network models. Environ Earth Sci 60:1037–1054

Raines GL, Sawatzky DL, Bonham-Carter GF (2010) Expert Knowledge: New fuzzy logic tools in ArcGIS 10. www.esri.com

RCMRD (2022) Uganda 30 meters SRTM Digital Elevation ModelUganda 30 meters SRTM Digital Elevation Model https://opendata.rcmrd.org/datasets/rcmrd::uganda-srtm-dem-30-meters/about (Accessed 15/07/2022)

Regmi NR, Giardino JR, McDonald EV, Vitek JD (2014) A comparison of logistic regression-based models of susceptibility to landslides in western Colorado, USA. Landslides 11(2):247–262

Roller S, Wittmann H, Kastowski M, Hinderer M (2012) Erosion of the Rwenzori Mountains, East African Rift, from in situ-produced cosmogenic10Be. J Geophys Res Earth Surf 117(F3)

Rupke J, Cammeraat E, Seijmonsbergen A, Van Westen C (1988) Engineering geomorphology of the Widentobel catchment, Switzerland: a geomorphological inventory system applied to geotechnical appraisal of the slope stability. Eng Geol 26:33–68

Saha A, Gupta R, Arora M (2002) GIS-based landslide hazard zonation in the Bhagirathi (Ganga) valley, Himalayas. Int J Remote Sens 23(2):357–369

Sassen M, Sheil D, Giller KE, ter Braak CJ (2013) Complex contexts and dynamic drivers: understanding four decades of forest loss and recovery in an East African protected area. Biol Conserv 159:257–268

Schlüter T (2008) Geological atlas of Africa (Vol. 307). Springer

Scott P (1998) From conflict to collaboration: people and forests at Mount Elgon. IUCN, Uganda

Sema HV, Guru B, Veerappan R (2017) Fuzzy gamma operator model for preparing landslide susceptibility zonation mapping in parts of Kohima Town, Nagaland, India. Model Earth Syst Environ 3:499–514

Silalahi FES, Arifianti Y, Hidayat F (2019) Landslide susceptibility assessment using frequency ratio model in Bogor, West Java, Indonesia. Geosci Lett 6(1):1–17

Simonetti A, Bell K (1995) Nd, Pb and Sr isotopic data from the Mount Elgon volcano, eastern Uganda-western Kenya: implications for the origin and evolution of nephelinite lavas. Lithos 36(2):141–153

Snyder NP, Whipple KX, Tucker GE, Merritts DJ (2000) Landscape response to tectonic forcing: Digital elevation model analysis of stream profiles in the Mendocino triple junction region, northern California. Geol Soc Am Bull 112(8):1250–1263

Soeters R, Van Westen CJ (1996) Slope instability recognition, analysis and zonation. Landslides Investig Mitig 247:129–177

Spudich P, Hellweg M, Lee W (1996) Directional topographic site response at Tarzana observed in aftershocks of the 1994 Northridge, California, earthquake: implications for mainshock motions. Bull Seismol Soc Am 86(1B):S193–S208

Styron R, Pagani M (2020) The GEM global active faults database. Earthq Spectra 36(1):160–180

Sykes LR (1967) Mechanism of earthquakes and nature of faulting on the mid-oceanic ridges. J Geophys Res 72(8):2131–2153

Sykes LR, Landisman M (1964) The seismicity of east Africa, the Gulf of Aden and the Arabian and Red Seas. Bull Seismol Soc Am 54(6A):1927–1940

Tangestani M (2004) Landslide susceptibility mapping using the fuzzy gamma approach in a GIS, Kakan catchment area, southwest Iran. Aust J Earth Sci 51(3):439–450

Tanyaş H, Van Westen CJ, Allstadt KE, Anna Nowicki Jessee M, Görüm T, Jibson RW, Godt JW, Sato HP, Schmitt RG, Marc O (2017) Presentation and analysis of a worldwide database of earthquake-induced landslide inventories. J Geophys Res Earth Surf 122(10):1991–2015

Taylor RG, Mileham L, Tindimugaya C, Mwebembezi L (2009) Recent glacial recession and its impact on alpine riverflow in the Rwenzori Mountains of Uganda. J Afr Earth Sc 55(3–4):205–213

Torizin J (2011) Bivariate statistical method for landslide susceptibility analysis using ArcGIS. Project of technical cooperation 'mitigation of georisks'. BGR-Report publication, Hannover

Towhata I, Wang G, Xu Q, Massey C (2022) Coseismic Landslides: phenomena, Long-term Effects and Mitigation. Springer Nature

UBoS (2022) Statistical Abstract. Ministry of Finance, Planning and economic development, The Government of Uganda, 14

UNESCO (1966) Earthquake reconnaissance mission, Uganda, the Toro earthquake of 20 March 1966. UNESCO. http://unesdoc.org/images/0000/000077/007799EB.pdf (Accessed 24/08/2022)

USGS (2010) Significant earthquakes of the world, 1994. United States Geological Survey. http://earthquake.usgs.gov/earthquakes/eqarchives/significant/sig_1994.php (Accessed 24/08/2022)

USGS (2022a) Digital Elevation Model (DEM) https://earthexplorer.usgs.gov/ (Accessed 15/07/2022)

USGS (2022b) Repository of Earthquake-triggered Ground-failure Inventories https://usgs.maps.arcgis.com/apps/webappviewer/index.html?id=2b6f1e57135f41028ea42ebc6813d967 (Accessed 23/07/2022)

Valagussa A, Marc O, Frattini P, Crosta GB (2019) Seismic and geological controls on earthquake-induced landslide size. Earth Planet Sci Lett 506:268–281

Van Eynde E, Dondeyne S, Isabirye M, Deckers J, Poesen J (2017) Impact of landslides on soil characteristics: Implications for estimating their age. CATENA 157:173–179

Van Westen C, Rengers N, Soeters R (2003a) Use of geomorphological information in indirect landslide susceptibility assessment. Nat Hazards 30:399–419

Van Westen C, Rengers N, Soeters R (2003b) Use of geomorphological information in indirect landslide susceptibility assessment. Nat Hazards 30(3):399–419

Vlaeminck P, Maertens M, Isabirye M, Vanderhoydonks F, Poesen J, Deckers S, Vranken L (2016) Coping with landslide risk through preventive resettlement. Designing optimal strategies through choice experiments for the Mount Elgon region Uganda. Land Use Policy 51:301–311

Wald DJ, Allen TI (2007) Topographic slope as a proxy for seismic site conditions and amplification. Bull Seismol Soc Am 97(5):1379–1395

Wanasolo I (2012) Assessing and mapping people's perceptions of vulnerability to landslides in Bududa. Uganda Norges teknisk-naturvitenskapelige universitet, Fakultet

Wang F, Cheng Q, Highland L, Miyajima M, Wang H, Yan C (2009) Preliminary investigation of some large landslides triggered by the 2008 Wenchuan earthquake, Sichuan Province, China. Landslides 6(1):47–54

Warr LN, Cox S (2001) Clay mineral transformations and weakening mechanisms along the Alpine Fault, New Zealand. Geol Soc Lond Spec Publ 186(1):85–101

Weatherill GA (2014) OpenQuake Hazard Modeller's Toolkit—User Guide. Global Earthquake Model (GEM). Technical Report

Weiss A (2001) Topographic position and landforms analysis. Poster presentation, ESRI user conference, San Diego, CA

Westerhof AB, Härmä P, Isabirye E, Katto E, Koistinen T, Kuosmanen E, Lehto T, Lehtonen MI, Mäkitie H, Manninen T (2014) Geology and geodynamic development of Uganda with explanation of the 1: 1,000,000 scale geological map. Geological survey of Finland

Whipple KX (2004) Bedrock rivers and the geomorphology of active orogens. Annu Rev Earth Planet Sci 32:151–185

Wieczorek G, Gori P, Jager S, Kappel W, Negussey D (1996) Assessment and management of landslide hazards near the Tulley Valley landslide, Syracuse, New York. Landslides, USA

WorldBank GFDRR (2022) Global Landslide Hazard Map. Data Catalog https://datacatalog.worldbank.org/search/dataset/0037584 (Accessed 27/07/2022)

WorldBank (2019) Disaster risk profile: Uganda https://documents.worldbank.org/en/publication/documents-reports/documentdetail/324521574236798679/disaster-risk-profile-uganda

Xu C (2015) Preparation of earthquake-triggered landslide inventory maps using remote sensing and GIS technologies: principles and case studies. Geosci Front 6(6):825–836

Yalcin A (2008) GIS-based landslide susceptibility mapping using analytical hierarchy process and bivariate statistics in Ardesen (Turkey): comparisons of results and confirmations. CATENA 72(1):1–12

Yilmaz I (2009) Landslide susceptibility mapping using frequency ratio, logistic regression, artificial neural networks and their comparison: a case study from Kat landslides (Tokat—Turkey). Comput Geosci 35(6):1125–1138

Zadeh LA (1965) Fuzzy sets. Inf Control 8(3):338–353

Zhuang J, Peng J, Iqbal J, Liu T, Liu N, Li Y, Ma P (2015) Identification of landslide spatial distribution and susceptibility assessment in relation to topography in the Xi'an Region, Shaanxi Province, China. Front Earth Sci 9:449–462

Zimmermann HJ (2012) Practical applications of fuzzy technologies. Springer Science and Business Media, Springer, Cham

Authors and Affiliations

Morris Oleng[1,2,3] · **Zuhal Ozdemir[1]** · **Kypros Pilakoutas[1]**

✉ Morris Oleng
wotamuko@gmail.com

Zuhal Ozdemir
z.ozdemir@sheffield.ac.uk

Kypros Pilakoutas
k.pilakoutas@sheffield.ac.uk

[1] Department of Civil and Structural Engineering, The University of Sheffield, Sheffield, UK

[2] Department of Civil and Environmental Engineering, Kyambogo University, Kampala, Uganda

[3] Department of Engineering and Environment, Uganda Christian University, Mukono, Uganda